Evolution of the lower Badenian depositional system in the East Slovakian Basin: Implications for reservoir rock potential

VIKTÓRIA SUBOVÁ[1,✉], SAMUEL RYBÁR[1,3], KATARÍNA ŠARINOVÁ[2], NATÁLIA HUDÁČKOVÁ[1], MICHAL JAMRICH[1] , ĽUBOMÍR SLIVA[4], BRANISLAV ŠÁLY[4] and IVAN HLAVATÝ[4]

[1]Department of Geology and Paleontology, Faculty of Natural Sciences, Comenius University in Bratislava, Mlynská dolina, Ilkovičova 6, 842 15 Bratislava, Slovakia; ✉ subova25@uniba.sk
[2]Department of Mineralogy, Petrology and Economic geology, Faculty of Natural Sciences, Comenius University in Bratislava, Mlynská dolina, Ilkovičova 6, 842 15 Bratislava, Slovakia
[3]Technical University of Ostrava, Faculty of Mining and Geology, Department of Geodesy and Mine Surveying, 17. listopadu 2172/15, 708 00 Ostrava Poruba, Czech Republic
[4]Nafta a.s., 821 09 Bratislava, Slovakia

Abstract: The Transcarpathian Basin, consisting of the Prešov and Trebišov sub-basins, is situated at the border of the Western and Eastern Carpathians. Hydrocarbon exploration in this basin has been ongoing for more than 60 years and reserves of economic importance are located in the E to NE part of the basin. The Trebišov sub-basin was analysed to characterize and predict lower Badenian (Langhian) reservoir rocks. To achieve this aim, new sedimentary facies, seismic facies, petrographic and paleontological analyses were performed, combined with original total porosity and permeability measurements. Based on the planktic foraminifera and calcareous nannoplankton zonation, the lower Badenian sequence in the Trebišov sub-basin was divided into a lower and an upper interval. The presence of very well sorted sandstone layers, glauconite grains, albitization, selective alteration of tuffs into zeolites as well as the fossil assemblages reinforce the volcanic influenced marine environments. Documented sedimentary structures indicate subaqueous density flows preceded by the newly observed fluvial and deltaic facies. The total sandstone porosity measurements indicate a gradual porosity decrease with depth marked by a value of 13.21 % at the surface decreasing down to 6.41 % at ~3 km below the surface. These numbers correspond to reservoirs with low to reduced porosity. Diagenetic products such as illite, chlorite and feldspar cement together with compaction effects, and variations in the crystallinity in siliceous cement led to the modification of initial porosity. The potential lower Badenian reservoir sandstones are frequently deformed by strike-slip faults responsible for the large pull-apart basin complex (seen as horsetail structures on reflection seismic sections) forming various fault-bounded structural traps. The lower Badenian sandstones present at the top of two anticlinal structures in the central part of the basin, display very strong reflection amplitudes on newly merged 3D reflection seismic data underlining the additional exploration potential in the basin.

Keywords: East Slovakian Basin, basin analysis, porosimetry, reservoir sandstones

Introduction

The East Slovakian Basin represents a significant depocenter with a total sediment thickness of 8–9 km (Vass et al. 2000). The basin is about 80 km wide and 90 km long and represents a part of the larger Transcarpathian Basin. The Slanské vrchy Mountains, create a distinct intra-basinal morphostructure, and divide the basin into two partial sub-basins: the **Trebišov** and the **Prešov** sub-basins. According to Vass (2002) the southern part of the East Slovakian Basin continues into the Moldava sub-basin, and to the valley of the Roňava River, which genetically belongs to the Nyírség Basin (Fig. 1). The history of hydrocarbon exploration and drilling in the East Slovakian Basin has lasted more than 60 years (Rudinec 1969b; Franců et al. 1989; Vass et al. 2005; Hlavatý et al. 2009; Milička et al. 2011). This resulted in the drilling of hundreds

of deep wells. However, outside of mostly confidential well reports, petrophysical properties (porosity and permeability) were poorly documented. Many kilometres of 2D seismic lines were shot and supplemented by 3D seismic volumes. During the recent cooperation of Aspect Ltd. and NAFTA Ltd., all 3D volumes were reprocessed and merged.

Hydrocarbon reservoirs of producing and economic importance are mostly located in the eastern and north-eastern parts of the basin. The reservoirs mostly evince a high porosity and are composed of sandy mudstones, medium- to coarse-grained sandstones and conglomerates (Rudinec 1976). Liquid hydrocarbons (light crude oil – gas condensate) were found practically in all extraction horizons. Outside of hydrocarbon fields, the basin also includes several carbon-dioxide (Vass et al. 2005) and geothermal reservoirs (Jacko et al. 2021). In most natural gas deposits, the mechanism of their trapping is based
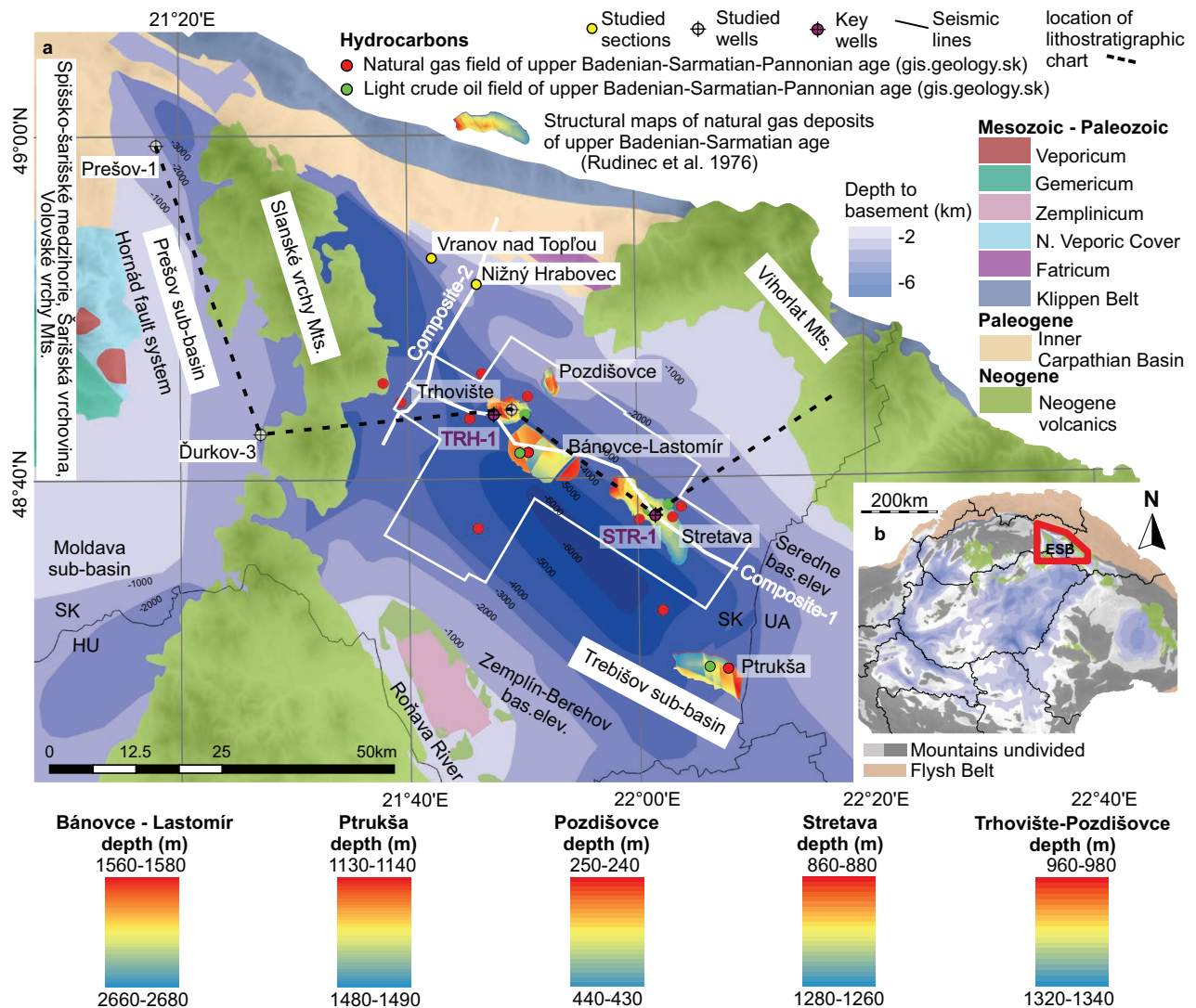
Fig. 1. Map of the East Slovakian Basin with the location of natural gas and light crude oil fields. Colour bars below the map represent depth izolines of producing fields. Modified after Fusán et al. (1987), Horváth at al. (2015), Hók et al. (2014), Biela (1978), Vranovská et al. (2012), Rudinec (1965, 1960).

on one major fault system. Therefore, it was possible to single out areas with significant gas deposits, including Ptrukša, Trhovište–Pozdišovce, Stretava–Senné and Bánovce structures (Fig. 1; Rudinec 1976; Vass et al. 2005). The gas production is highly dependent on lithology, and it ranges from several thousand Nm³/24 hours to more than 1 million m³/24 hours. Pressure in the deep reservoirs (2400–4000 m) is up to 90 % higher than hydrostatic pressure and the temperature ranges between 140–210 °C (Vass et al. 2005). Reservoir pressures decrease to 5–40 % above the hydrostatic pressure in the shallow depths (0–2400 m) and the temperature decreases to less than 140 °C. The total gas reserves of the basin were calculated to 5.8×10^9 m³. The extracted reserves represent about 4.2×10^9 m³, and so the residual reserves may represent up to 1.6×10^9 m³ (Vass et al. 2005). Other estimates (Boote et al. 2018) calculated the total reserves in the East Slovakian Basin as 63 Million Barrels of Oil Equivalent (MMboe).

With respect to the future, discovery of new reservoirs could improve the energy self-sufficiency of Slovakia.

The reservoirs in the Stretava and Trhovište gas structures (Fig. 2) are fragmented by several faults, which may indicate a predisposition to structural trap formation. Moreover, the Stretava structure includes gas horizons both of the lower Badenian (~3000 m) and Sarmatian age (~1300–1200 m). The Trhovište–Pozdišovce structure holds gas pools with a small capacity of lower Badenian (~2900 to 2700 m) and also of late Badenian age (~1300 to 800 m; Rudinec 1976). The lower Badenian sedimentary facies and associated reservoirs in these two wells (Stretava-1 and Trhovište-1 well) have not been extensively studied and thus never fully understood. Therefore, the aim of this study is to analyse the lower Badenian (Langhian) depositional environments of the East Slovakian Basin. Special attention is paid to the recognition and prediction of potential reservoirs within them.
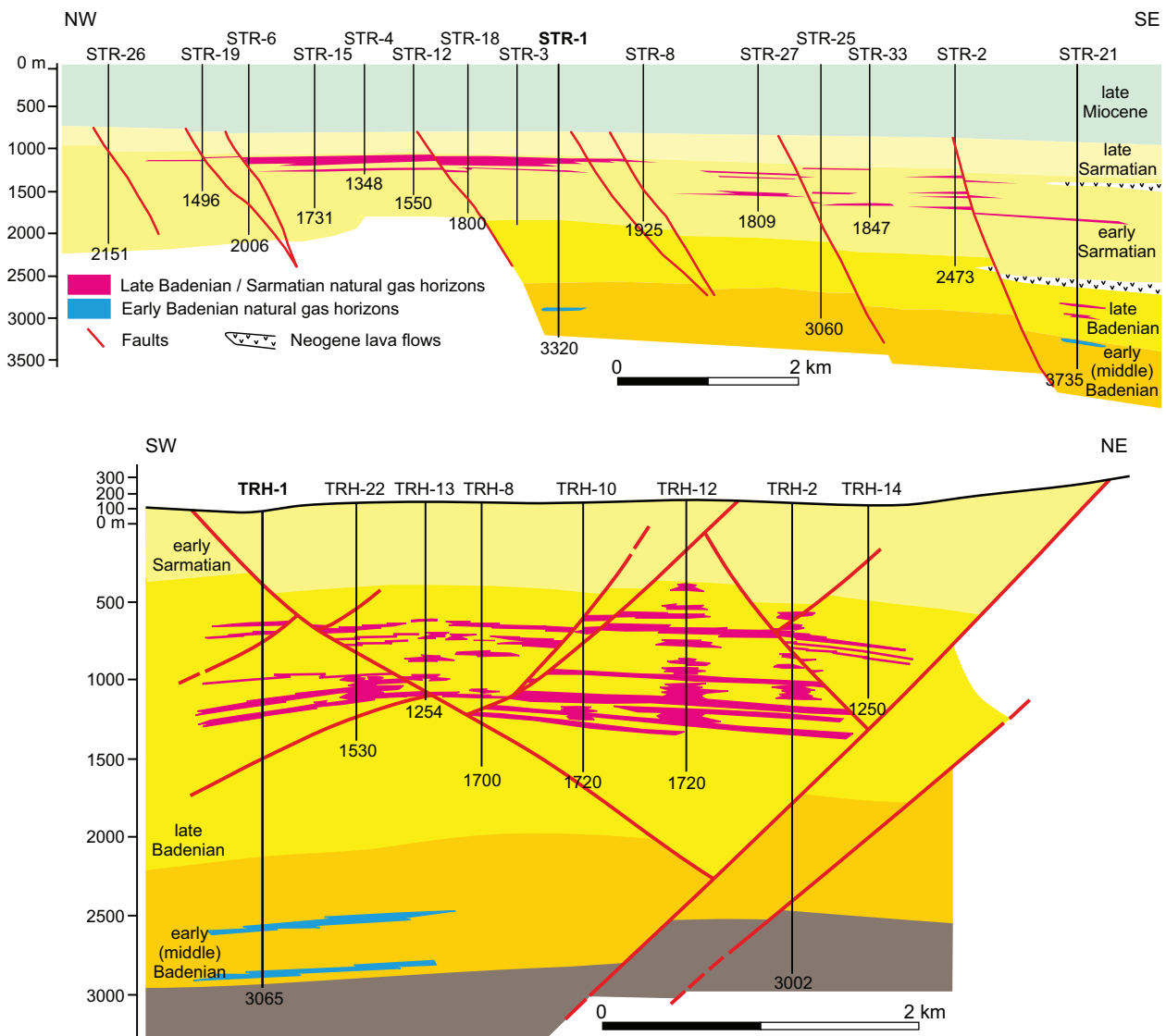
Fig. 2. Geological cross-sections with projected wells across the Stretava and Trhovište structures. Natural gas horizons are highlighted in pink and blue. Modified after Rudinec (1976).

Geological settings

Two different models that account for the tectono-sedimentary evolution of the East Slovakian Basin were proposed. The first model (Kráľ et al. 1990; Vass et al. 2005; Vass 1998, 2002) proposes that the deposition started in a compressional basin that preceded the East Slovakian Basin sensus stricto, which developed close to the subduction zone of the Outer Carpathians. The sedimentation in this basin probably took place from the Paleogene up to the Eggenburgian. Subsequently, this basin was partially eroded during the Ottnangian. The second model (Baráth et al. 1997; Kováč & Zlinská 1998; Kováč 1999, 2000) also interpreted a compressional regime during the Egerian–Eggenburgian–Ottnangian stage and described the basin as a "basin on an active continental margin". Thus, according to the terminology of Allen & Allen (2013),

this could be labelled as a foreland basin. With respect to the Karpatian stage, the first model (Kráľ et al. 1990; Vass et al. 2005; Vass 1998, 2002) interpreted the onset of an extensional to transtensional regime, which lasted until the middle Sarmatian. The basin is declared to be a pull-apart due to the following reasons: high surface heat flow density (Franko et al. 1995), thinned lithosphere, anisotropic basin basement with elements of oceanization, basin opening by strike-slip faults with flower structures, "en-echelon" faults, pronounced volcanic activity, rapid subsidence connected to great thickness of clastic sediments, and migration of the depocenter from NW to SE. Vass (2002) and Vass et al. (2005) claim that in the middle of the Badenian stage, the pull-apart regime was paused due to a salinity crisis (Zbudza Formation). The second model (Baráth et al. 1997; Kováč & Zlinská 1998; Kováč 1999, 2000) agrees with the onset of rifting in a pull-apart basin but

postulates that the deposition occurred during the Karpatian and early Badenian only. During the late Badenian and Sarmatian stages, the basin is declared to have opened through back-arc extension controlled by subduction zone roll-back known from the other parts of the Pannonian Basin (Tari et al. 1992). The Pannonian interval according to the first model (Kráľ et al. 1990; Vass et al. 2005; Vass 1998, 2002) was elaborated only marginally, and the tectonic regime was labelled as extensional. According to the second model (Baráth et al. 1997; Kováč & Zlinská 1998; Kováč 1999, 2000), the Pannonian interval is characterized by a shift into post-rift thermal subsidence in an "intermontane basin". Both models (Kráľ et al. 1990; Vass et al. 2005; Vass 1998, 2002; Baráth et al. 1997; Kováč & Zlinská 1998; Kováč 1999, 2000) agree with the onset of a compressional regime connected with basin inversion in between the Pontian to Pliocene stages (Fig. 3).

The pre-Cenozoic basement of the East Slovakian Basin is very heterogeneous. For consistency, the work of Fusán et al. (1987) is followed. In the north, the basement rocks belong to mostly Mesozoic rocks of the Pieniny Klippen Belt and are rimmed by Mesozoic and Permian rocks of the Fatric Nappe (Hók et al. 2014). In the west, the basement is formed by the Mesozoic and upper Paleozoic Tatric and Veporic cover units of the Western Carpathians. The South-West is occupied by Paleozoic crystalline schists of the Veporic unit and by Paleozoic rocks of the Gemeric unit (Hók et al. 2014). South from the Gemeric unit Mesozoic rocks appear and are assigned to the Meliatic, Silicic and Turnaic units (Vass 2002; Hók et al. 2014). The central part of the basin together with the eastern and southern margin is occupied by Mesozoic and Paleozoic rocks of the "Potisie block" (Fusán et al. 1987) today better known as the Zemplinicum unit (Hók et al. 2014). In the south, a minor patch of crystalline schists is assigned to the Zemplinicum unit as well (Vass 2002; Hók et al. 2014).

The Paleogene sediments are mainly concentrated in the northern and central parts of the basin and occupy a variety of units (Rudinec 1980). North from the Pieniny Klippen Belt the Paleogene sediments belong to the Magura unit and south of the Klippen Belt the Paleogene sediments are associated with the Inner Carpathian Paleogene Basin. Minor Paleogene rocks may be present in the south-west and are assigned to the Hungarian Paleogene Basin (Tari et al. 1993; Vass 2002; Hók et al. 2014).

The Neogene fill is occupied by sedimentary and volcano-sedimentary formations of the Eggenburgian (lower Burdigalian) up to the late Miocene time. The Neogene strata are covered by Quaternary deposits (Fig. 3; Vass 2002; Vass et al. 2005).

The formations of the **Eggenburgian age** (lower Burdigalian) are made up of the Prešov and Čelovce formations (fms.; Vass 2002). The Prešov Formation (Fm.) is composed of calcareous sandy siltstones with layers of fine calcareous sandstones, and altered rhyolite tuff (Vass 2002). The Čelovce Fm. includes alternations of siltstones, claystones, fine-grained sandstones and conglomerates. The **Ottnangian** strata (middle Burdigalian) have not been recorded, and thus have

possibly been eroded (Vass 2002). The **Karpatian** (upper Burdigalian) formations are composed of the Teriakovce Formation, which is built by conglomerates, mudstones and tuffs (Vass 2002). The Soľná Baňa Fm. follows and includes salt breccias with crystalline halite, and unsorted chaotic, sharp-edged fragments of claystones and sandstones. Sandy laminated anhydrites are also present (Karoli in Kaličiak 1991; Vass 2002). The Karpatian deposition ends with the Kladzany Fm., which contains variegated sandy-claystones and clays (Leško 1955; Matějka et al. 1964; Vass & Čverčko 1985; Vass 2002). The **Badenian** strata (Langhian–lower Serravallian) begin with the Nižný Hrabovec Fm. composed of calcareous sandstone, siltstone and claystone with layers of conglomerates, and with local gypsum concretions (Slavík 1953; Matějka et al. 1964; Vass & Čverčko 1985; Vass 2002). A zeolitized tuff, known as the Hrabovec tuff (Kuthan 1948; Matějka et al. 1964) forms the lower interval of this formation (Vass 2002). The Vranov Fm. consists of grey calcareous siltstones, claystones and sandstones. The discrimination factor between the Nižný Hrabovec Fm. and the Vranov Fm. is the absence of the tuffs (Vass 2002). The Zbudza Fm. includes clays and evaporite layers, represented by halite, anhydrite and gypsum (Janáček 1959; Vass & Čverčko 1985; Karoli 1998). The Mirkovce Fm. is formed by grey calcareous claystones and acidic volcanics (Kaličiak 1991; Vass 2002). The Lastomír Fm. is composed of calcareous clays–claystones with layers of sand, and acidic tuffs (Matějka et al. 1964; Vass & Čverčko 1985; Vass 2002). The younger formations are not significant for the aims of this study and the reader is referred to Janáček (1959), Brodňan et al. (1959), Čverčko et al. (1969), Rudinec & Čverčko (1970), Vass & Čverčko (1985) and Vass (2002).

Methodology

For this study a review of existing literature (e.g., Rudinec 1978, 1989; Vass 2002; Vass et al. 2005), and original well reports (Rudinec 1960, 1965, 1969a, b, 1975 and 1976) has been done. Well core samples were obtained in the Gbely core repository of NAFTA Ltd. petroleum company. For the purpose of the lithological and sedimentological description well core samples were cut in half perpendicular to the bedding plane and digitized. Lithofacies were described according to Bouma et al. (1985), Miall (2006), Nielsen et al. (2007), Talling et al. (2012) and Rossi et al. (2017; Table 1). Basic well logs (spontaneous potential and resistivity) were evaluated according to Rider & Kennedy (2011). Seismic and sequence stratigraphy interpretations mainly followed the works of Brown & Fischer (1980), Coe (2003), Fischer & Veeken (2015).

Standard thin sections were studied under a polarizing microscope and analysed by electron microprobe. Selected thin sections were stained by alizarin red pigment which changes the colour of $CaCO_3$ to red. Coarse-grained samples, tuffs and tuffites were analysed under the Cameca SX 100
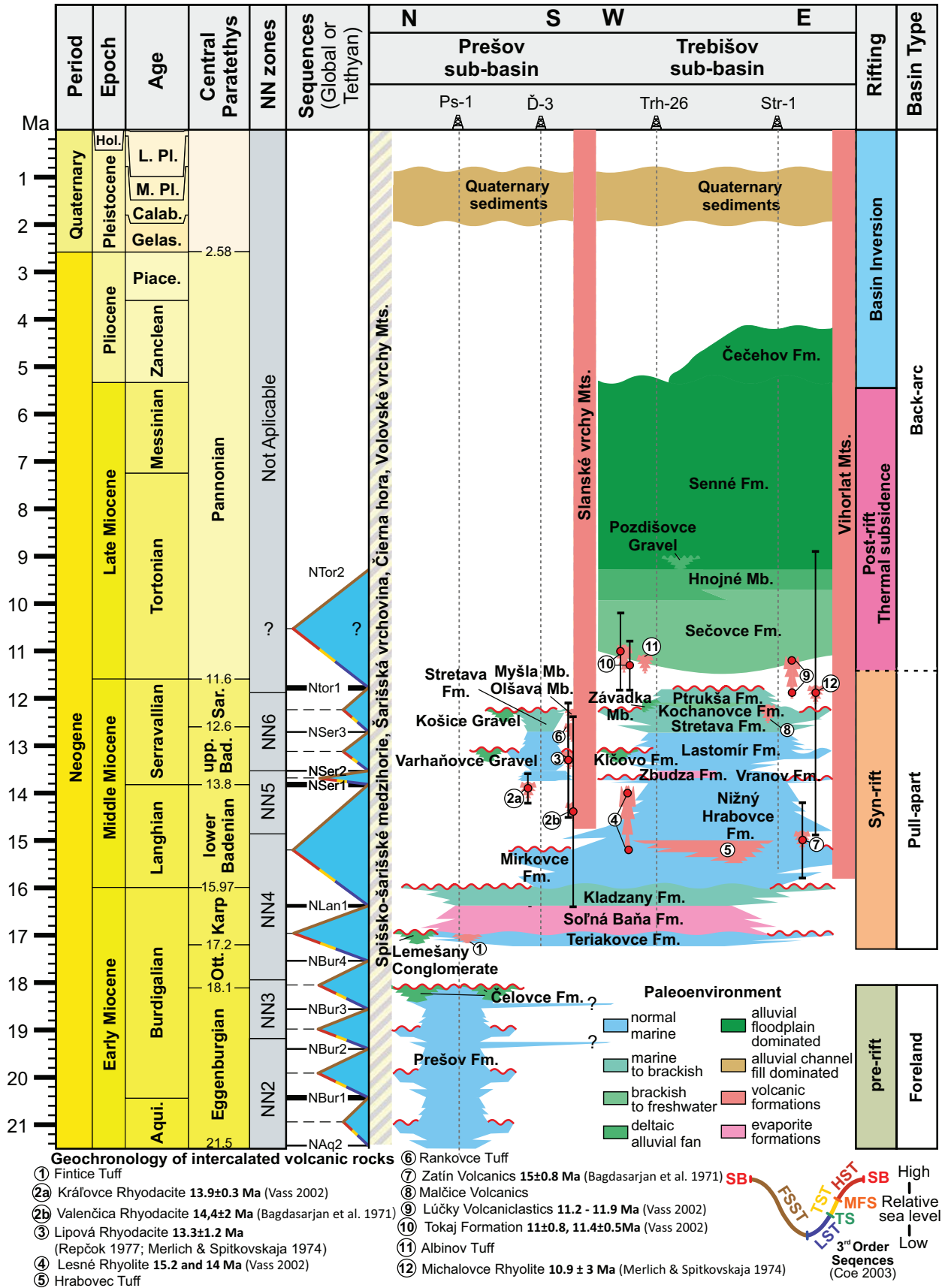
Fig. 3. Lithostratigraphic table of the East Slovakian Basin. Modified after Kováč (2000); Vass (2002); Vass et al. (2005) and Kováč et al. (2007, 2018).

Table 1: Lithofacies table modified after Miall (2006), Németh & Martin (2007); Talling et al. (2012) and Rossi et al. (2017).

Lithofacies code	Lithofacies association code	Lithofacies description		Depositional process and paleoenvironment	Interpretation of dep. process association
Miall (2006); Németh & Martin (2007)		Sediment. texture	Sediment. structure	Rossi et al. (2017); Németh & Martin (2007)	
Gm	Gm+Fs+ Spl+Sg	Matrix supported gravel	Soft-sediment deformation	Fluvial dominated	Fluvial dominated/ inner shelf
Spl		Sand, fine	Plane-parallel lamination	Fluvial and tide dominated	
Sg		Sand, fine	Graded	Event beds, fluvial dominated	
Fs		Silt, clay	Massive	Ephemeral lake with rare marine ingressions, suspension	
Ct/ Ctr		Zeolitized coarse tuff/ redep. tuff	Massive	Pyroclastic deposit/ redeposited pyroclastic deposit	Volcanic middle shelf
Talling et al. (2012)				Talling et al. (2012)	
Sm	Ta	Ta+Tb	Sand, very fine to coarse	Massive, faint lamination, bioturbation	Massive sand formed incrementally via deposition from traction carpet	High density turbidite
Sl	Tb		Sand, very fine to coarse	Rhytmic lamination	Planar laminated sand formed in dilute flow by low amplitude bed-waves	
Sr	Tc	Tc+Te	Sand, very fine to coarse	Ripple-cross lamination	Ripple cross-laminated sand deposited by dilute fully turbulent flow	Low density turbidite
Fm	Te		Silt, clay	Massive and/or laminated	Massive mud deposited from gel with network of bonds (?)	

microprobe (State Geological Institute of Dionýz Štúr). Minerals were identified using WDS analysis with accelerating voltage 15 keV, probe current 20 nA, with a beam diameter of 10 μm. Additionally, the presence of anhydrite was confirmed by Raman spectroscopy (Slovak Academy of Sciences). Total porosity measurements of coarse-grained rocks by the mercury injection method (Dandekar 2013) were performed in the Unichema Ltd. laboratory. Porosity values are presented based on the classification systems by Khanin (1965, 1969) and Koesoemadinata (1980).

Foraminifera have been obtained from 100 g of well core material, which was diluted by hydrogen peroxide and wet sieved (0.071 and 1 mm). The binocular stereoscopic microscope (Olympus SZ75) and the biological polarizing microscope were used for the determination of foraminifera and the scanning electron microscope QUANTA FEG 250 was used for their imaging (Institute of Electrical Engineering, SAS). The obtained residua were split into approximately 300 specimens (if possible). Determination of foraminifers is based on Loeblich & Tappan (1992), Cicha et al. (1998), Łuczkowska (1974) and Holbourn et al. (2013). Due to the poor preservation of the foraminiferal tests, some stay in open nomenclature. The biostratigraphic assignment is in accordance with Cicha et al. (1998) and Iaccarino et al. (2011).

Calcareous nannofossils were studied from smear slides prepared by the following standard methods of sample preparation for quantitative analysis (Bown 1998). Samples were analysed using an Olympus BX50 microscope at 1250× magnification. Camera Olympus Infinity 2, with Quick PHOTO CAMERA 2.3 software was used for the photographic record. Specimens were counted at 300 fields of view (FOV) using a quantitative method. Systematic identification of calcareous

nannofossils was done using the taxonomy of Young (1998) and Young et al. (2017). Standard nannofossil NN zonation (Martini 1971) was used for age determination.

Results

Nižný Hrabovec section (NHQ; description)

The Nižný Hrabovec section (Table 2) is situated in a zeolite quarry east of Nižný Hrabovec village (Fig. 4). The quarry is actively mined for zeolite, and it consists of six quarry levels. In the given time the studied sediments were located on the 3rd and 4th level, above the zeolitized Nižný Hrabovec tuff, at the right part of the quarry (see Fig. 4b). An eleven-metre-high sedimentological section was constructed on the 4th level (Fig. 4c).

With respect to lithology, the lowermost layer of the section is formed by a grey-green massive coarse-grained zeolite (Ct/ Ctr; sample HPS-1; Figs. 4c, 5; see Table 1 for all following lithofacies code) with a thickness from 0 to 1.6 m of the section, which extends downwards deeper into the quarry. Above, the zeolite (sample NHQ-1; Fig. 5) alternates with

Table 2: Coordinates of the studied sections and wells.

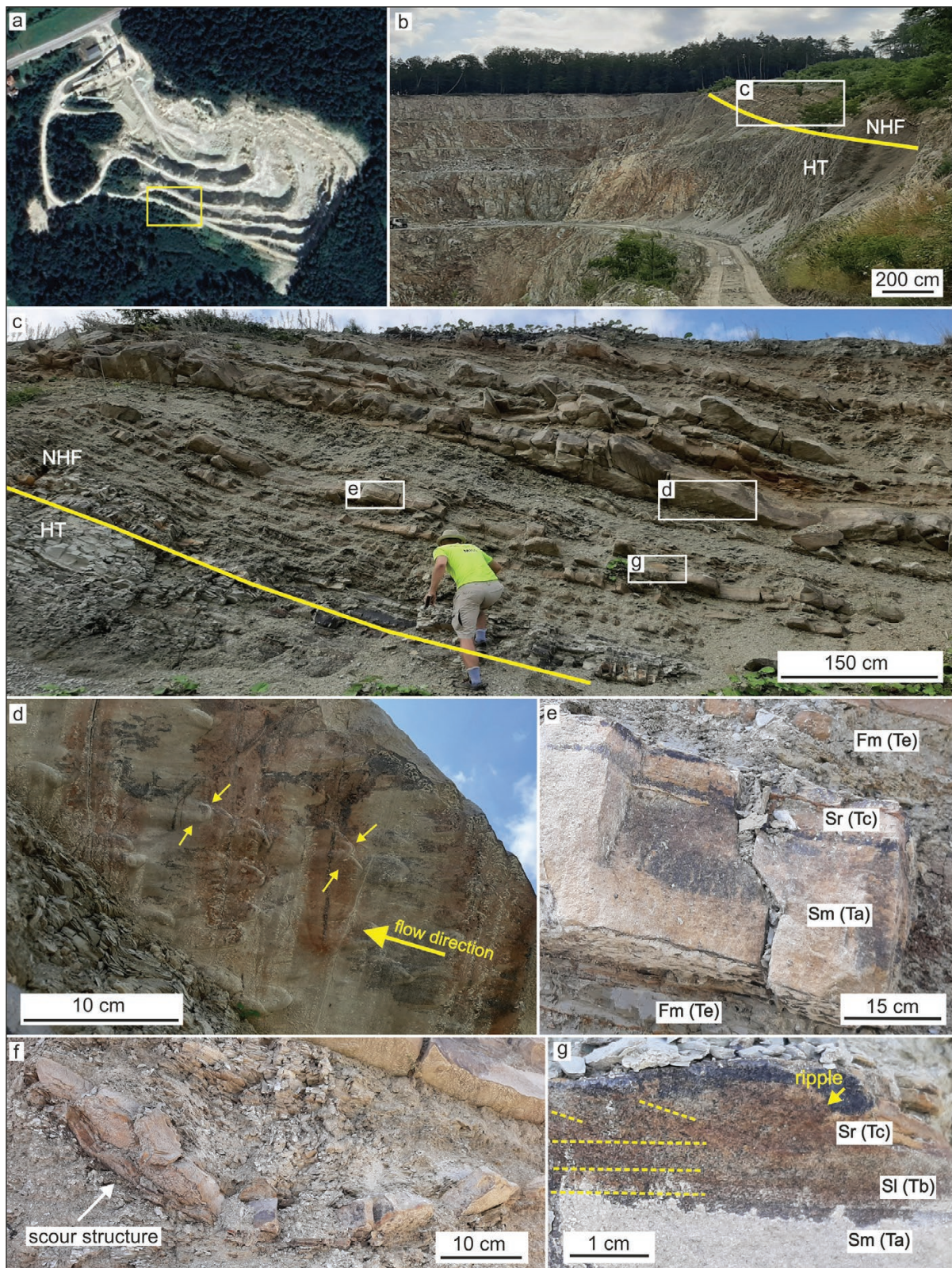| Well / section	WGS 84 decimal		WGS 84 decimal	
	x	y	Longitude	Latitude
STR-1	22.024689	48.63043	22°01'28.882"E	48°37'49.561"N
TRH-1	21.790501	48.72911	21°47'25.804"E	48°43'44.822"N
NHQ	21.767988	48.85799	21° 46'4.755"E	48°51'28.770"N
VNT	21.698978	48.88355	21°41'56.319"E	48°53'0.809"N

Fig. 4. The Nižný Hrabovec section. **a** — Satellite map of the quarry with highlighted position of the studied section. **b** — View towards the individual levels of the quarry. The yellow line separates the Hrabovec Tuff (HF) from sandstones and mudstones of the Nižný Hrabovec Formation (NHF). The rectangle highlightes the studied profile. **c** — Detail of the studied section. **d** — Flutes and grooves at the base of the massive sandstones, arrow is showing the flow direction. **e** — Massive and ripple-cross laminated sandstone layers surrounded by massive mudstones. **f** — U-shaped channel structure surrounded by massive mudstones. **g** — Arrows show indistinct ripple-cross laminated sandstone layer. For the facies codes explanation see Table 1.
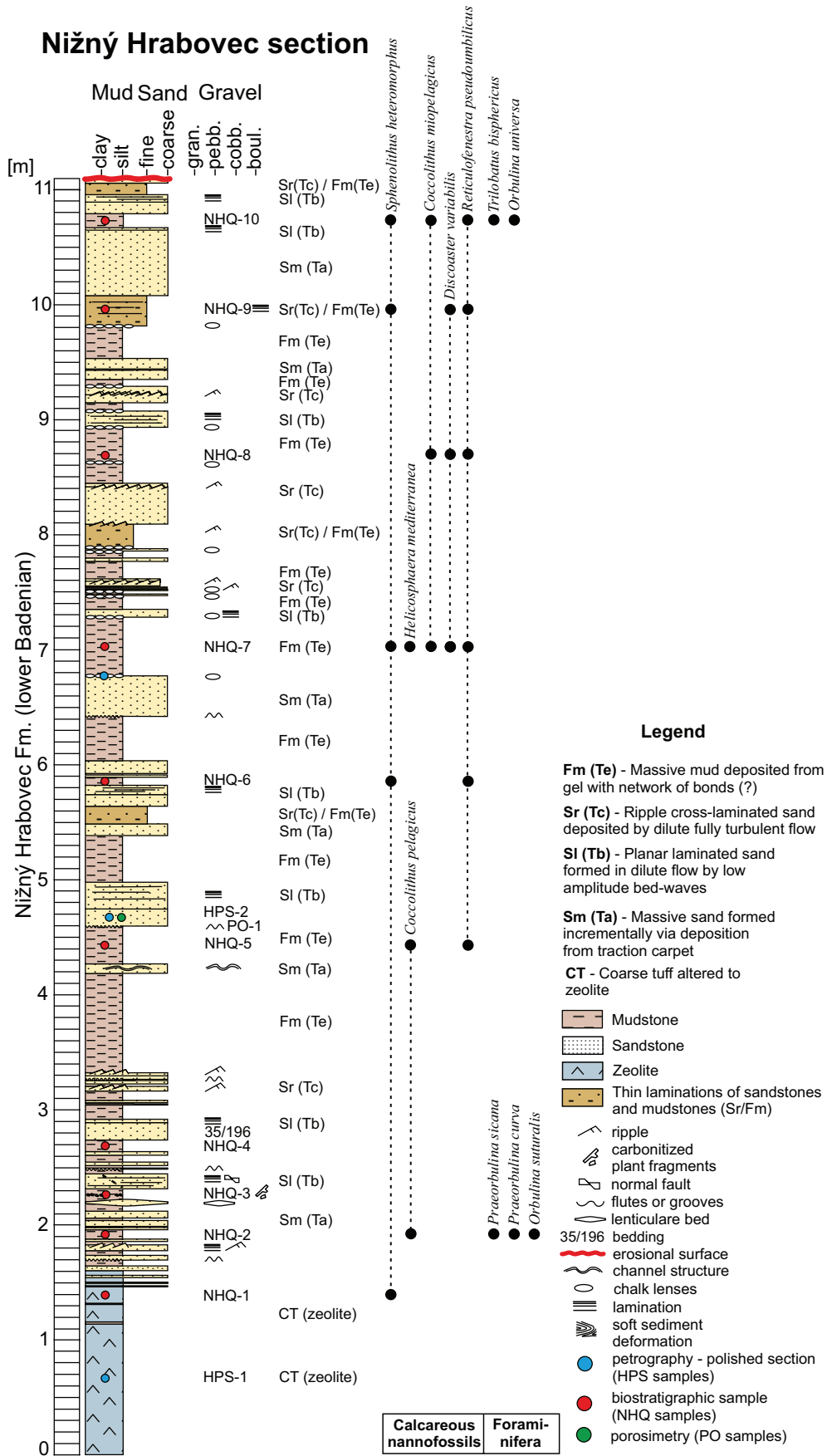
Fig. 5. Sedimentary profile of the lower Badenian Nižný Hrabovec section.

thin layers of massive mudstones (Fm-facies code explain in Fig. 4), and massive sandstones (Sm). In between the heights of 1.6 to 3.3 m in the section (Fig. 5), massive mudstones (Fm; NHQ-2, 3, 4) alternate with massive, laminated and ripple-cross laminated sandstones (Sm, Sl and Sr; Figs. 4e–g, 5). At the base of sandstones, flutes and grooves were commonly recognized (Fig. 4d). Occasionally the sandstones are arranged in lenticular beds and carbonatized plant fragments are common. Massive mudstones (NHQ-5) occur between 3.3 to 4.6 m of the section. Within this bed an 0.08 m thick massive sandstone (Sm) layer is present. The cross section of the sandstone bed is U-shaped and resembles a scour (Figs. 4f, 5). In between 4.6 to 6.8 m of the section, alternation of massive, laminated sandstones (Sm and Sl), and massive mudstones (Fm) follow. In between 5.5 to 5.65 m of the section, the facies change to thin laminated sandstones and mudstones. At the base of massive sandstones (Sm), flute marks and grooves are present. Due to a low degree of alteration at around 4.7 m of the section, a sample for porosimetry (sample PO-1; Fig. 5), and a sample for petrography (HPS-2) was taken. At around 5.8 m a mudstone sample (NHQ-6) was obtained. In between 6.8 to 9.8 metres of the section, massive, laminated, ripple-cross laminated sandstones (Sm, Sl and Sr), and massive mudstones (Fm; NHQ-7, 8) are commonly intercalated by discontinuous white, "chalky" layers (1–2 cm in diameter). According to petrographic studies, these layers are formed by microsparite recrystallized from micrite. In between 9.8 to 11.1 metres of the section, white concretions are absent. The rest of the section is formed by massive, laminated, ripple-cross laminated sandstones (Sm, Sl and Sr) and massive mudstones (Fm; NHQ-9, 10). At the height of 11.1 metres, the section ends with an erosional surface, which is covered by recent soil (Fig. 5).

Zeolites were originally crystallovitroclastic fine-grained tuffs with max. clast diameter of 0.25 μm. Crystalloclasts are made up of Pl, Bt, Qz, Ap and Zrn. Glass shards and pumice fragments are fully replaced by zeolites. These results are in accordance with previous studies (Tschegg et al. 2019, 2020). In addition to Tschegg et al. (2019, 2020), K-feldspars are predominantly authigenic and fill in empty spaces in zeolitized glass fragments, and they also form reaction rims on the contact between plagioclase and zeolitized glass (Figs. 6a, 7b; Supplement S1a). The amount of orthoclase molecule is high (Or$_{99.34–99.98}$; Fig. 8) and K-feldspars do not evince an ideal stoichiometry (Suppl. S1a).

The sandstones above zeolites are well sorted (Fig. 7a), but the grains are dominantly angular to subangular. The grain composition consists of mono- and polycrystalline quartz, K-feldspar, relatively fresh plagioclase (albite), muscovite, felsite/chert, glauconite, siltstone, phyllite to schist clasts, volcanic clasts, and heavy minerals (rutile, garnet, zircon, Fe-oxy /hydroxides, xenotime). In more weathered samples, glauconite is altered to Fe oxides. Upward, the content of micritic carbonate grains and fossil shells increase together with local carbonate cement. Predominant siliceous cement has different degrees of crystallization (from amorphous to crystalline).

Siliceous cement contains Al, Fe, Ca and K admixture (Fig. 6b; Suppl. S1c). Some grains show hematite rims. Moreover, authigenic K-feldspar is present in the form of idiomorphic crystals, and also in the form of overgrowths around detrital K-feldspars (Fig. 6c; Suppl. S1a).

Ten biostratigraphical samples (NHQ-1 to NHQ-10) were taken (Fig. 5). The foraminifera association was very poorly preserved, mostly only the molds were retained. Despite the preservation, it was possible to identify stratigraphically significant species of planktic foraminifera (Fig. 9; Suppl. S3): *Trilobatus bisphericus* (sample NHQ-10; Fig. 9a)*, Praeorbulina curva (*NHQ-2; Fig. 9c)*, Praeorbulina sicana* (NHQ-2; Fig. 9b)*, Orbulina universa* (NHQ-10; Fig. 9i)*, Orbulina suturalis (*NHQ-2; Fig. 9d–h). It is necessary to note that only planktic foraminifera were found and benthic taxa were missing. Stratigraphically significant calcareous nannofossils were also abundant in this section (Fig. 10; Suppl. S3): *Sphenolithus heteromorphus* (Fig. 5, NHQ-10, 9, 7, 6, 1; Fig. 10a, b), *Coccolithus miopelagicus* (Fig. 5, NHQ-10, 8, 7; Fig. 10e–g), *Reticulofenestra pseudoumbilicus* (Fig. 5, NHQ-10, 6, 5; Fig. 10h), *Discoaster variabilis* (Fig. 5, NHQ-9, 8, 7; Fig. 10f), *Helicosphaera mediterranea* (Fig. 5, NHQ-7; Fig. 10d) and *Coccolithus pelagicus* (Fig. 5, NHQ-5, 2; Fig. 10c).

Vranov nad Topľou section (description)

The Vranov nad Topľou section (Table 2) is located on a road cut above the church in Vranov nad Topľou town (Fig. 11a). This locality shows sediment of the Vranov Formation (Vass 2002).

Two sedimentological profiles were constructed (P1 and P2; Fig. 11b, 12) with a total height of 3.8 m. Between 0 and 0.8 m of the P1 section, massive sandstones (Sm; see Table 1 for all following lithofacies code) and massive mudstones (sample VNT-1; Fm) alternate with thinly laminated sandstones and mudstones (Sr/Fm; Fig. 11d). At the height of 80 cm, the layer of massive mudstones (Fm) is terminated by a discontinuity (Fig. 11c). Between 0.8 and 1.8 metres of the section, the sedimentation continues with alternations of massive sandstones (Sm), massive mudstones (Fm; VNT-2), and thinly laminated sandstones together with mudstones (Sr/Fm; VNT-3). The P1 section can be laterally connected with the P2 section (Fig. 12). Between 1.8 and 3.6 m of the composite section, thin laminations of sandstones and mudstones (Sr/Fm; VNT-4) follow. Between 3.6 and 3.8 metres, layers of massive sandstones (Sm), and massive mudstones (Fm) appear once again. At the height of 3.8 metres, the composite section ends with an erosional surface, which is covered by recent soil (Figs. 11b, 12).

Laminated sandstones from the section (sample VPS-1) are well sorted with subangular grains. In composition monocrystalline quartz, and altered feldspar dominate. They are accompanied by felsites/cherts, muscovite, glauconite, phyllite, and micrite grains. Chalcedon spherulite fragments and fossils (foraminifera) are rare. The cement is predominantly formed
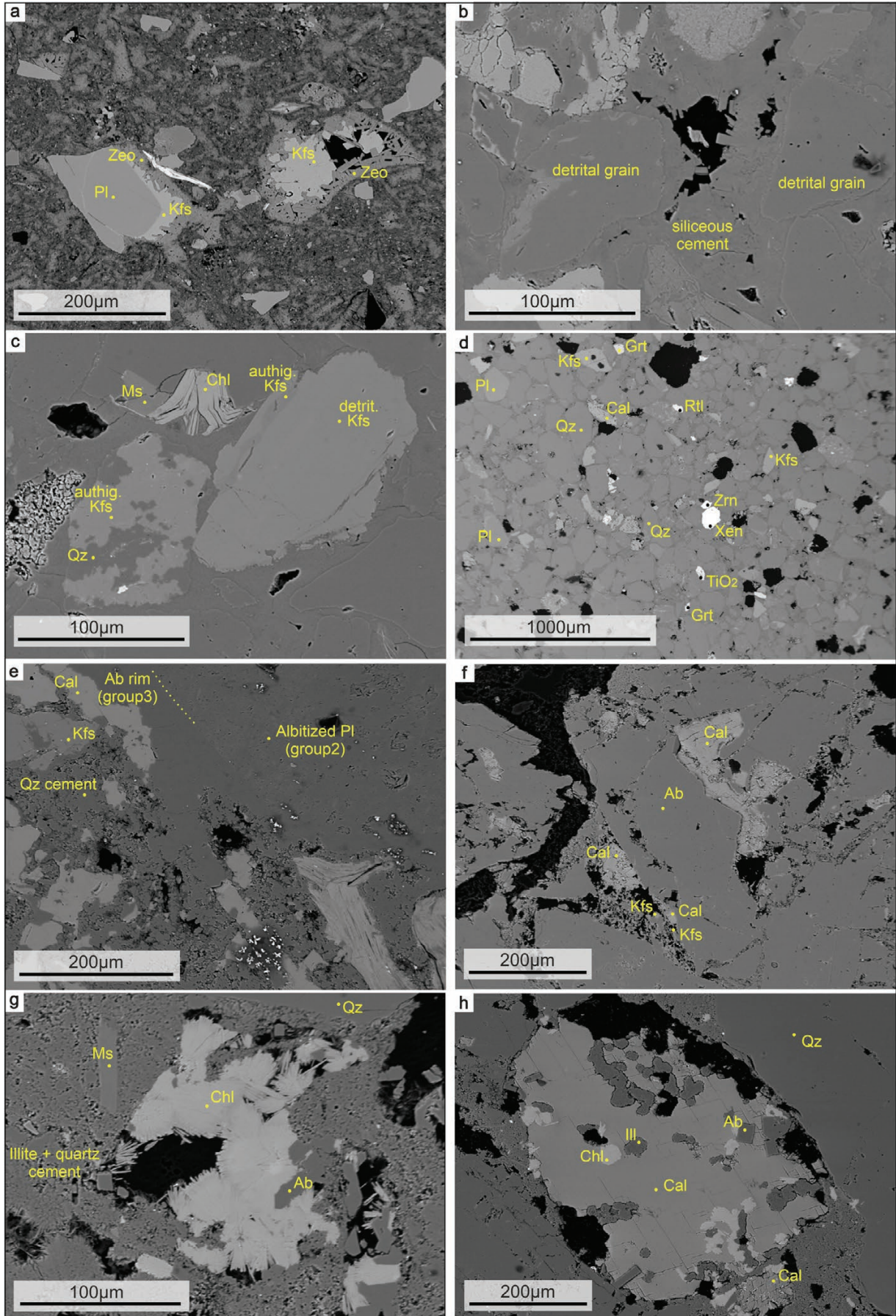
Fig. 6. BSE images: **a** — Authigenic K-feldspars in pore space and in reaction rim between plagioclase crystaloclasts and zeolitized glass. Original glass shards are replaced by zeolite minerals (zeolite; the Nižný Hrabovec section (NHQ)); **b** — Crystals of siliceous cement (sandstone; NHQ); **c** — Idiomorphic shape of the authigenic K-feldspar in Si cement and K-feldspar overgrowths around detrital K-feldspars (sandstone; NHQ); **d** — Well sorted sandstone with siliceous cement, composed of K-feldspar, quartz, plagioclase, calcite, garnet, rutile, xenotime and zircon (sandstone; NHQ); **e** — Albite rim (group3) around albitized detrital plagioclase (group2) with micropores. The groundmass is formed by siliceous cement and final calcite cement (sandstone; TRH-1 well; 3007–3012 m); **f** — Authigenic K-feldspar- and calcite crystals along the edge of detrital, fully albitized plagioclase; calcite cement fill intragranular, secondary pore in plagioclase (sandstone; STR-1; 3054–3060 m). The extra porosity is most likely a result of tearing during thin section assembly and polishing; **g** — Idiomorphic crystals of albite and needle-shaped chlorite as pore-filling cement in illite and quartz cemented sandstone. The shape and size of the pore is similar to the shape and size of detrital grains, indicating dissolution or replacement of a detrital grain (sandstone; STR-1; 3054–3060 m); **h** — Diagenetic chlorite, illite and albite enclosed by calcite cement. The shape and size of the calcite crystal is similar to the shape and size of detrital grains, indicating dissolution or replacement of a detrital grain (sandstone; STR-1; 3054–3060 m).

by calcite crystals (locally poikilitic) to a less extend by dolomite crystals (Fig. 7c, d). The cement is additionally coloured by secondary diagenetic ferric oxides.

Four biostratigraphical samples were taken from the massive mudstone layer (VNT-2; Fig. 12) and from thin laminations of sandstones and mudstones (Fig. 12, VNT-1, 3, 4; Suppl. S4). Foraminifera tests were very poorly preserved occasionally recrystallized and sometimes overgrown by crystals. Nevertheless, it was possible to identify stratigraphically significant species of planktic foraminifera e.g. (Fig. 9): *Orbulina suturalis* (Fig. 12, VNT-1, 2, 4;), *Globigerina druryi* (Fig. 12, VNT-4), *Globigerina ciperoensis* (Fig. 9j, VNT-4), *Globorotalia bykovae* (Fig. 9k, VNT-4), *Valvulineria complanata* (Fig. 9l–m, VNT-1), *Melonis pompilioides* (Fig. 9n, VNT-2), *Bulimina elongate* (Fig. 9o, VNT-4), *Bolivina* sp. (Fig. 9p, VNT-2), *Uvigerina grilli* (Fig. 9q, VNT-2), *Ammonia parkinsoniana* (Fig. 9r, VNT-1), *Elphidium macellum* (Fig. 9s, VNT-1), *Textularia gramen* (Fig. 9t, VNT-1), *Bogdanowiczia pocutica* (Fig. 9u, VNT-1) and *Rhizammina algaeformis* (Fig. 9v, VNT-1). The samples also contain abundant redeposited species from the lower Miocene, Oligocene (Figs. 9, 12, VNT-4) and Cretaceous (Figs. 9, 12, VNT-2). Clasts in the washed residue were well rounded, included glauconite and echinoid spines. It was also possible to identify stratigraphically important calcareous nannofossils (Figs. 10, 12; Suppl. S4): *Sphenolithus heteromorphus* (Fig. 12, VNT-1, 3, 4; Fig. 10i), *Coronocyclus nitescens* (elliptical; Fig. 12, VNT-2, 3; Fig. 10j)*, Discoaster exilis* (Fig. 12, VNT-3, 4; Fig. 10k) and *Helicosphaera wallichii* (Fig. 12, VNT-4; Fig. 10l).

Trhovište-1 (TRH-1) well (description)

The total depth of the Trhovište-1 well is 3067.6 metres (Fig. 13; Table 2). The well includes 38 well-core samples, but only some of them were available in the repository. The sediments were studied from core samples and additional information was explored from the original well report (Rudinec 1960).

With respect to the basic well logs (SP- spontaneous potential and RT- resistivity), the Trhovište-1 well is divided as follows. In the interval between 3037–2649 m (core-37 to 30; Fig. 13), the SP log displays symmetrical and funnel trends with pronounced high negative excursions, especially

correlating with the core-36, 32, 31 and 30. The SP log in the following interval of 2649–2299 m (core-29 to 23) shows cylindrical and symmetrical trends with high amplitude negative deflections. The highest excursions correlate with core-29, 28 and core-27; Fig. 13).

From the sedimentological point of view, it can be stated that in the depth of 3059–3056 m (core-38; Figs. 13, 14a), the cores are composed of grey to dark brown, massive, calcareous mudstones (Fm; see Table 1 for all following lithofacies code) with white clasts (~1 to 2 mm in diameter). In the depth of 3034–3031 m (core-37a; Fig. 14b) dark brown, massive calcareous mudstones (Fs) are present. The interval of 3012–3007 m (core-37; Fig. 14c) is represented by grey-green, coarse-grained tuffites and volcanic mudstones (Ct/Ctr). Sediments in the depth of 2971–2946 m (core-36; Fig. 14d) consist of dark brown, massive mudstones (Fs). The interval between 2902–2649 m (core-35, 34, 33, 32; Rudinec 1960), is formed by tuff, redeposited tuff (Ct/Ctr), claystones and calcareous sandstones, which continue towards overburden. In the depth of 2711–2697 m (core-31; Fig. 14e) light, grey redeposited tuffs (Ct/Ctr) are present. In 2652–2649 m (core-30; Fig. 14f) grey-green, fine-grained, massive volcanic tuffs/redeposited tuff (Ct/Ctr) are included. In the depth of 2601–2499 m (core-29, Fig. 14g; 28, 27) brown, massive sandstones (Sm) and carbonatized plant fragments occur. Between 2452–2250 m (core-26, 25, 24, 23, 22), sediments are made up of alternations of brown, massive mudstones (Fm), and thin layers of sandstones. Carbonatized plant fragments may occur.

With respect to the aim of the study coarse-grained samples were selected for petrographic analyses. It was noted that in the depth of 3059–3056 m (core-38), the detrital grains are represented by quartz, feldspar and mica in carbonate-clay matrix, which is partially recrystallized. Additionally, according to the results from the Raman spectroscopy white nodules are filled by anhydrite and chalcedony (Fig. 15a). In the depth of 3012–3007 m (core-37; Fig. 15b, c), the sandstone is rich in plagioclase, quartz, biotite replaced by chlorite, spherulite fragments, magmatic corroded quartz, and altered volcanic glass. Plagioclase show different degrees of albitization, and thus it was possible to divide them into 3 groups (Suppl. S1a). The first group consists of oligoclase (anorthite molecule An_{20-28}; Fig. 8), which reflects the character of volcanism. The second group is characterized by variable anorthite content (An_{4-10}), shows microporosity (Fig. 6e) and documents progressive
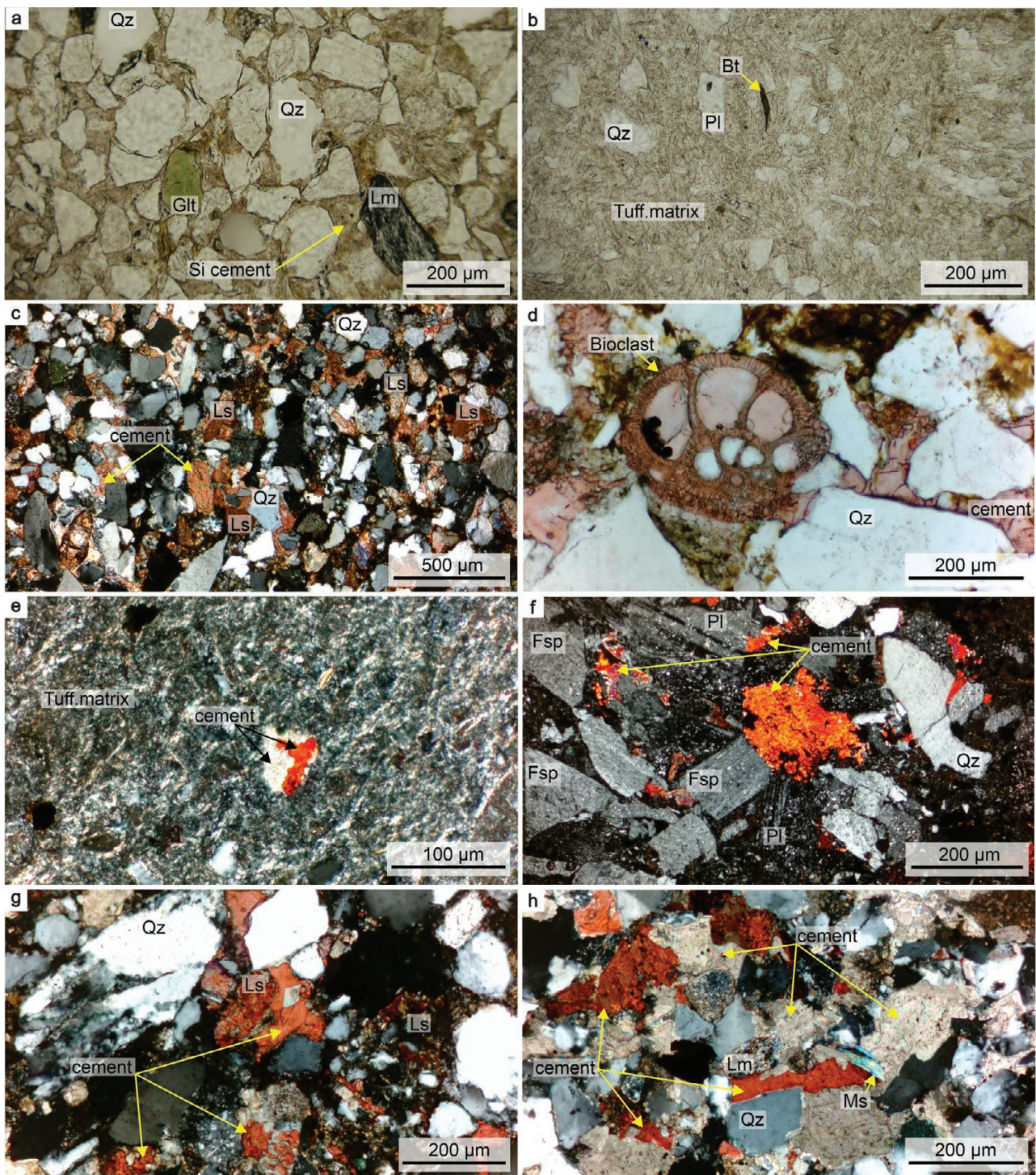
Fig. 7. Thin sections analysed under polarizing microscope. Core = C; Box = B; depth in m. The division of cement type was done by staining with alizarin red pigment; red colored grains/cement = calcite; uncolored = dolomite. **a** — Sorted sandstone composed of quartz (Qz), glauconite (Glt), metamorphic lithoclast (Lm) with Si-cement (NHQ section, HPS-2); **b** — Tuff with quartz (Qz), plagioclase (Pl) and biotite (Bt) in tuffitic matrix made up of zeolitized glass shards (NHQ section, HPS-1); **c** — Sorted sandstone built by sedimentary lithoclasts (Ls) and quartz (Qz) with a predominating calcite cement (VNT section, VPS-1); **d** — Sandstone with a stained foraminifera bioclast and quartz (Qz) in calcite cement (VNT section, VPS-1); **e** — Tuff composed of calcite, dolomite cement and tuffitic matrix (TRH-1, C30: 2649–2652, B3); **f** — Volcanic sandstone composed of feldspar (Fsp), plagioclase (Pl) and quartz (Qz) with predominating calcite cement (TRH-1, C31: 2697–2711, B4); **g** — Sandstone composed of sedimentary lithoclasts (Ls) and quartz (Qz) with predominating calcite cement (STR-1, C30: 2194–2200); **h** — Sandstone composed of metamorphic lithoclast (Lm), quartz (Qz) and muscovite (Ms) in equally distributed calcite and dolomite cement (STR-1, C45: 2950–2953, B3).
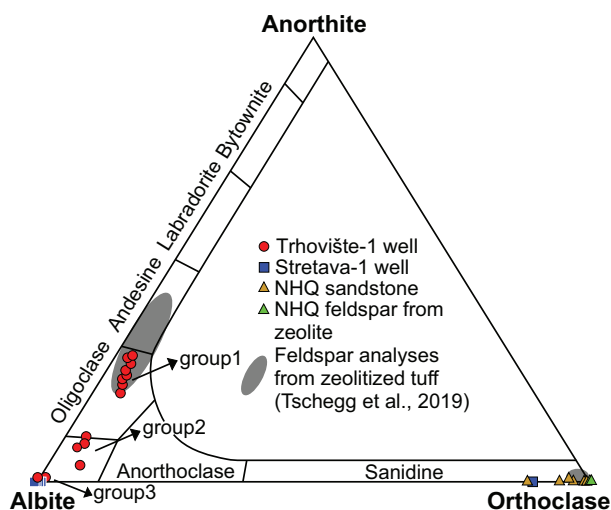
Fig. 8. Ternary plot of feldspar major elemental composition from the Nižný Hrabovec quarry based on probe analysis, TRH-1 (core-37) and STR-1 well (core-47).

albitization of detrital plagioclase. The third group represents the albite overgrowth (up to $An_{0.9}$) around detrital plagioclase together with albite crystals in the cement (Fig. 6e). Silica (Qz) cement dominates, calcite cement also occurs. Total porosity was measured in the core-37 with a value of 6.41 % (Table 3).

In the depth of 2711–2697 m (core-31; Figs. 7f, 15d), samples are composed of quartz, plagioclase, altered feldspar, volcanic clasts, and opaque minerals in tuffitic matrix. A sign of magmatic corrosion, which forms embayments and voids in quartz grains are sporadically observed. The porphyric volcanic clasts are rare. Tuffitic matrix is replaced by silica cement and calcite cement is occasionally also present. Detrital grains of non-volcanic origin consist of clay intraclasts and lithoclasts of sedimentary rocks (clayey carbonates with calcite veins). Bioclasts are also visible. In the depth of 2652–2649 m (core-30; Figs. 7e, 15e), detrital grains are represented by quartz, glauconite, altered biotite, and feldspar in tuffitic matrix.

Foraminifera associations were variably preserved (Suppl. S5). Only calcite molds were occasionally retained. Nevertheless, it was possible to identify some stratigraphically important species: *Orbulina suturalis, Praeorbulina glomerosa, Trilobatus trilobus, Trilobatus bisphericus* and *Globoturborotalita quinqueloba* (core-37, box-1); *Bogdanowiczia pocutica* (core-32, box-1).

Stretava-1 (STR-1) well (description)

The total depth of the Stretava-1 well is 3320 metres (Fig. 16). The well includes 52 well-cores and all of them were sampled. With respect to the basic well logs, the Stretava-1 well is divided in the following way (Fig. 16). Between 3320 and 3103 m (core-52 to 48), the SP log displays multiple symmetrical and funnel trends with pronounced negative

excursions. The highest excursion correlates with core-49. The RT log also displays high amplitudes with positive cylindrical, funnel and symmetrical trends. In the interval between 3103 and 3004 m (core-47 and 46), the SP log shows funnel and bell trends with negative excursions. The RT log reveals low amplitudes with positive symmetrical trends. In the interval from 2953 to 2605 m (core-45 to 38), the SP log displays high negative deflections with symmetrical trends. The RT log displays high amplitudes with positive predominantly symmetrical, bell and funnel trends.

From the sedimentological perspective, it is observed that in the depth of 3320–3317 m (core-52; Figs. 16, 17a), the fine-grained, green-grey-red coloured conglomerates (Gm; see Table 1 for all following lithofacies code) are altered and display soft sediment deformation. In the depth of 3253–3250 m (core-51), dark brown, massive mudstones (Fs) include plane-parallel sandy laminas (Spl), which may be graded (Sg). In the interval between 3202 and 3199 m (core-50; Fig. 17b, c), dark brown, massive mudstones continue with floating fine pebbles. Parallel laminated mudstones (Fm) alternate with massive fine sandstones (Sm) that include small erosional features at the base. Sediments in the depth of 3153–3151 m (core-49; Fig. 17d) consist of brown massive (Sm), laminated to graded sandstones (Sl). In the depth of 3105–3103 m (core-48) sediments are composed of dark brown, massive to laminated mudstones. Above at 3060–3054 m (core-47; Fig. 17e) and 3010–3004 m (core-46) grey, coarse-grained, massive sandstones (Sm) to fine conglomerates are present.

The depth intervals between 2953 and 2700 m (core-45, 44, 43, 42, 41, 40) include light brown, massive (Sm; see Table 1 for all following lithofacies code) to laminated sandstones (Sl) and dark brown, massive to laminated mudstones (Fm). In each core of this interval, sandstones predominate and are rich in pyrite concretions and carbonatized plant fragments. In the depth of 2953–2950 m (core-45; Fig. 17f, g) sandstones include mudstone intraclasts. Muddy sands occur for the first time in the depth of 2898–2895 m (core-44; Fig. 17h). In core-43 (2853–2850 m) sandy convolute ripple-cross (Sr) and parallel lamination (Sl) begin to appear. In the depth of 2761–2756 m (core-41; Fig. 17l) pronounced bioturbation is recognized. Sandstones from core-42 (2803–2800 m; Fig. 17k) and core-40 (2703–2700 m; Fig. 17m) are mostly normally graded or massive (Sm) and include faint lamination (Sl). In the depth of 2649–2646 m (core-39; Fig. 17n), and 2610–2605 m (core-38; Fig. 17o) brown, massive to laminated mudstones (Fm) alternate with ripple-cross, and convolute ripple-cross laminated sandstones (Sr). Muddy sandstones are also present.

From the petrographic point of view, the fine-grained conglomerate from the depth of 3320–3317 m (core-52) is composed of monocrystalline quartz, altered feldspar, bioclasts, and lithoclasts. Volcanic lithoclasts consist of plagioclase phenocrysts in felsite groundmass or fragments of chalcedony spherulites. Carbonate clasts, siltstone and mudstone grains also occur. Matrix is clayey-micritic, but carbonate cement and carbonatization of grains are also observed. In the depth
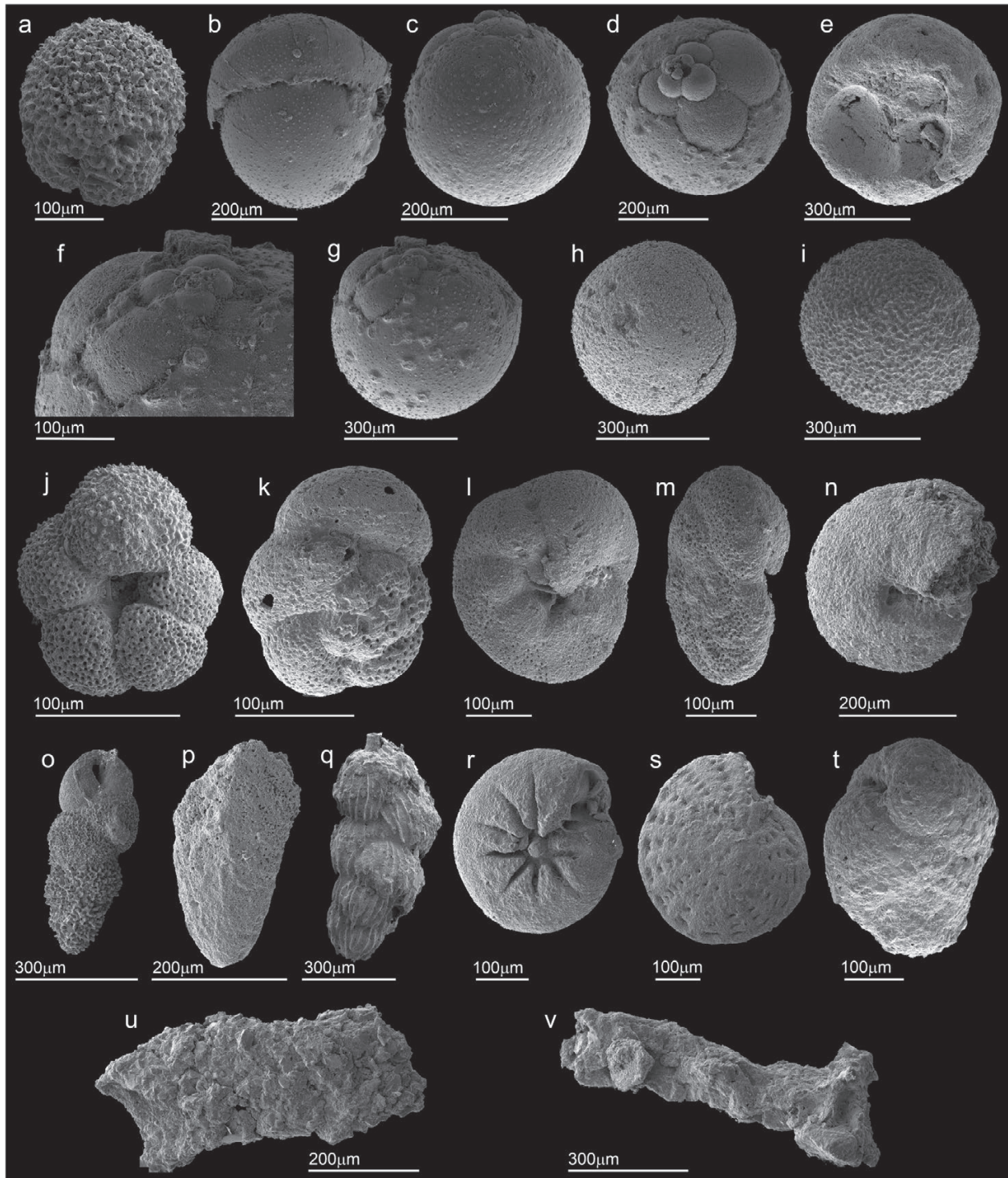
Fig. 9. Key foraminifera species from **(1)** the Nižný Hrabovec section (NHQ): **a** — *Trilobatus bisphericus,* Todd, 1984 – from the NHQ-10 sample*;* **b** — *Praeorbulina sicana* De Stefani, 1950 – from the NHQ-2 sample*;* **c** — *Praeorbulina curva* (Blow, 1956) – from the NHQ-2 sample*;* **d–h** — *Orbulina suturalis* Brönnimann, 1951 – from the NHQ-2 sample*;* **i** — *Orbulina universa* d'Orbigny, 1839 NHQ-10. **(2)** the Vranov nad Topľou section (VNT): **j** — *Globigerina ciperoensis* Bolli 1954 umbilical view – from the VNT-4 sample; **k** — *Globorotalia bykovae* Aisenstat 1960 spiral view – from the VNT-4 sample; **l** — *Valvulineria complanata* (d'Orbigny, 1846) umbilical view – from the VNT-1 sample; **m** — *Valvulineria complanata* (d'Orbigny, 1846) side view – from the VNT-1 sample; **n** — *Melonis pompilioides* (Fichtel & Moll, 1798) – from the VNT-2 sample; **o** — *Bulimina elongata* d'Orbigny, 1826 – from the VNT-4 sample; **p** — *Bolivina* sp. – from the VNT-2 sample; **q** — *Uvigerina grilli* Schmid, 1971 – from the VNT-2 sample; **r** — *Ammonia parkinsoniana* (d'Orbigny, 1839) umbilical view – from the VNT-1 sample; **s** — *Elphidium macellum* (Fichtel & Moll, 1798) – from the VNT-1 sample; **t** — *Textularia gramen* d'Orbigny, 1846 – from the VNT-1 sample; **u** — *Bogdanowiczia pocutica* Pishvanova, 1967 – from the VNT-1 sample; **v** — *Rhizammina algaeformis* Brady, 1879 – from the VNT-1 sample. For the location of the samples see Figs. 5 and 9.
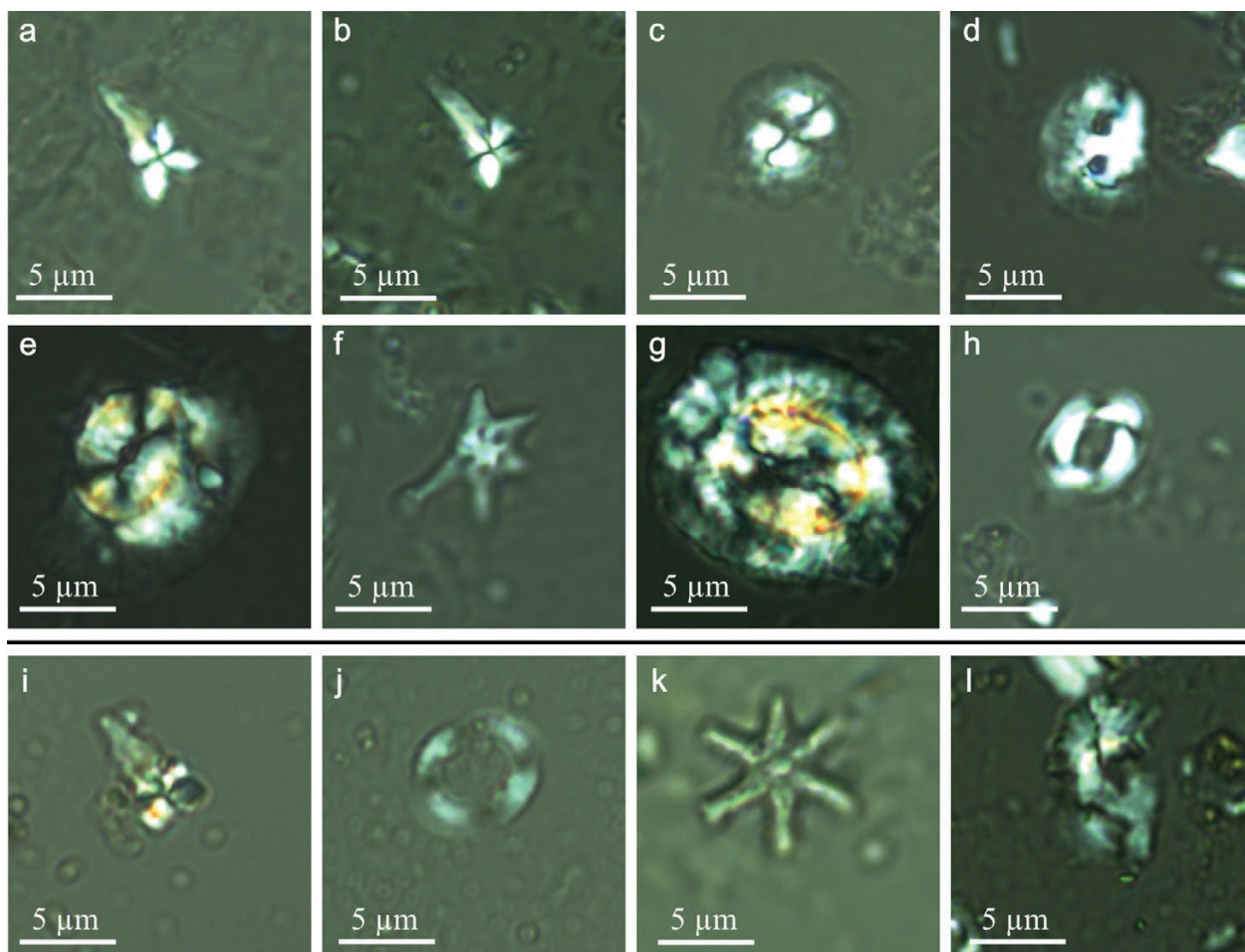
Fig. 10. Key calcareous nannofossil species from the Nižný Hrabovec and Vranov section. **NHQ**: **a, b** — *Sphenolithus heteromorphus* Deflandre, 1953 (NHQ-1, 7); **c** — *Coccolithus pelagicus* (Wallich, 1877) Schiller, 1930 (NHQ-5); **d** — *Helicosphaera mediterranea* Muller, 1981 (NHQ-7); **e, g** — *Coccolithus miopelagicus* Bukry, 1971 (NHQ-7, 8); **f** — *Discoaster variabilis* Martini and Bramlette, 1963 (NHQ-7); **h** — *Reticulofenestra pseudoumbilicus* (Gartner, 1967) Gartner, 1969 (NHQ-10). **VNT**: **i** — *Sphenolithus heteromorphus* Deflandre, 1953 (VNT-1); **j** — *Coronocyclus nitescens* (elliptical) (Kamptner, 1963) Bramlette and Wilcoxon, 1967 (VNT-2); **k** — *Discoaster exilis* Martini and Bramlette, 1963 (VNT-3); **l** — *Helicosphaera wallichii* (Lohmann, 1902) Okada and McIntyre, 1977 (VNT-4).

between 3202–3199 m (core-50) the floating pebbles are composed of large volcanic clasts (up to 2 cm in diameter; Fig. 15f), with porphyric texture in microcrystalline groundmass, which are often partially replaced by calcite. Phenocrysts are formed by altered plagioclase and quartz. Except for pebbly volcanic grains, mudstone consists of silt sized quartz, feldspar, and mica grains. The carbonate-clay matrix is recrystallized and locally carbonate cemented (or replaced by calcite?). The poorly sorted fine conglomerate in the depth of 3060–3054 m (core-47; Fig. 15g) consists of subangular grains of altered plagioclase, monocrystalline quartz with signs of magmatic corrosion, felsic and microlithic volcanic clasts, micrite and sparite grains. Mudstone clasts, biotite, sedimentary cherts, polycrystalline quartz and bioclasts are rare. Plagioclase is fully replaced by albite (group3; Fig. 8; Suppl. S1a). Authigenic K-feldspars occasionally crystallize along with fractures within plagioclases, and their crystals are also present at the edge of plagioclase (Fig. 6f). The ground-

mass is predominantly formed by siliceous and illite cement (Fig. 6g, h; Suppl. S1b, c). Authigenic needle-shaped chlorite together with albite, and calcite fill empty spaces (Fig. 6g; Suppl. S1b). Total porosity was measured in the core-47 with a value of 9.96 % (Table 3).

The sandstones from the interval of 2953-2950 m (core-45; Fig. 15h, to 40), are similar in composition. They are moderately sorted, detrital grains consist of subangular quartz, altered feldspar, volcanic rock fragments (felsites), mica, glauconite and bioclasts. Diagenetic minerals are present as siliceous, calcite and dolomite cement (Fig. 7h). From the lower to upper part sedimentary rock fragments such as carbonate grains and cherts are observed. In the depth of 2095–2100 m (core-38), sandstone is composed of quartz, biotite and plagioclase grains. Calcite cement forms a significant part of the studied samples.

Foraminifera samples were barren and only a poor calcareous nannofossil assemblage was recognized in the interval

Fig. 11. The Vranov nad Topľou section. **a** — Satellite map with the position of the road cut. **b** — Section with the studied profiles P1 and P2. **c** — Slump body in massive sandstones. **d** — Thin alternations of sandstones (Sr) and mudstones (Fm).
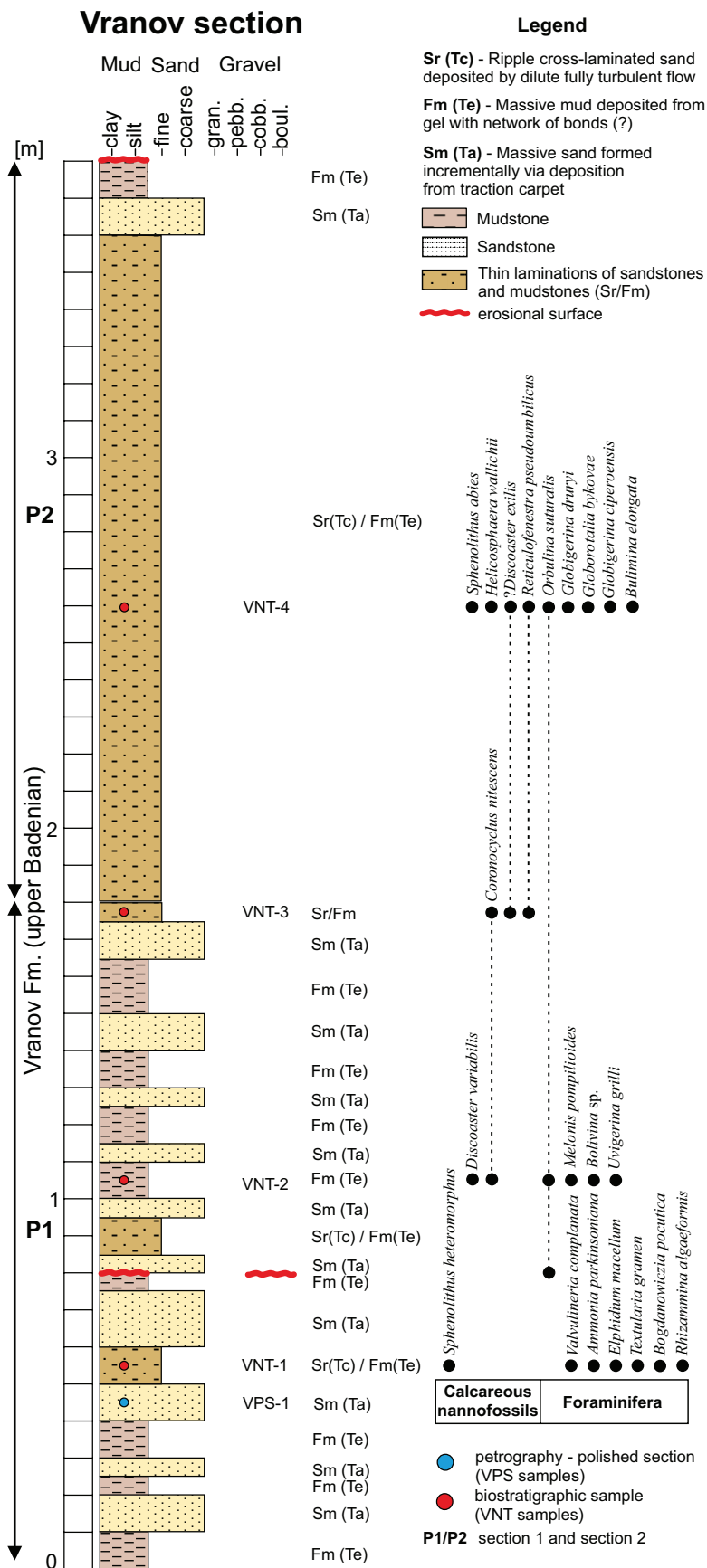
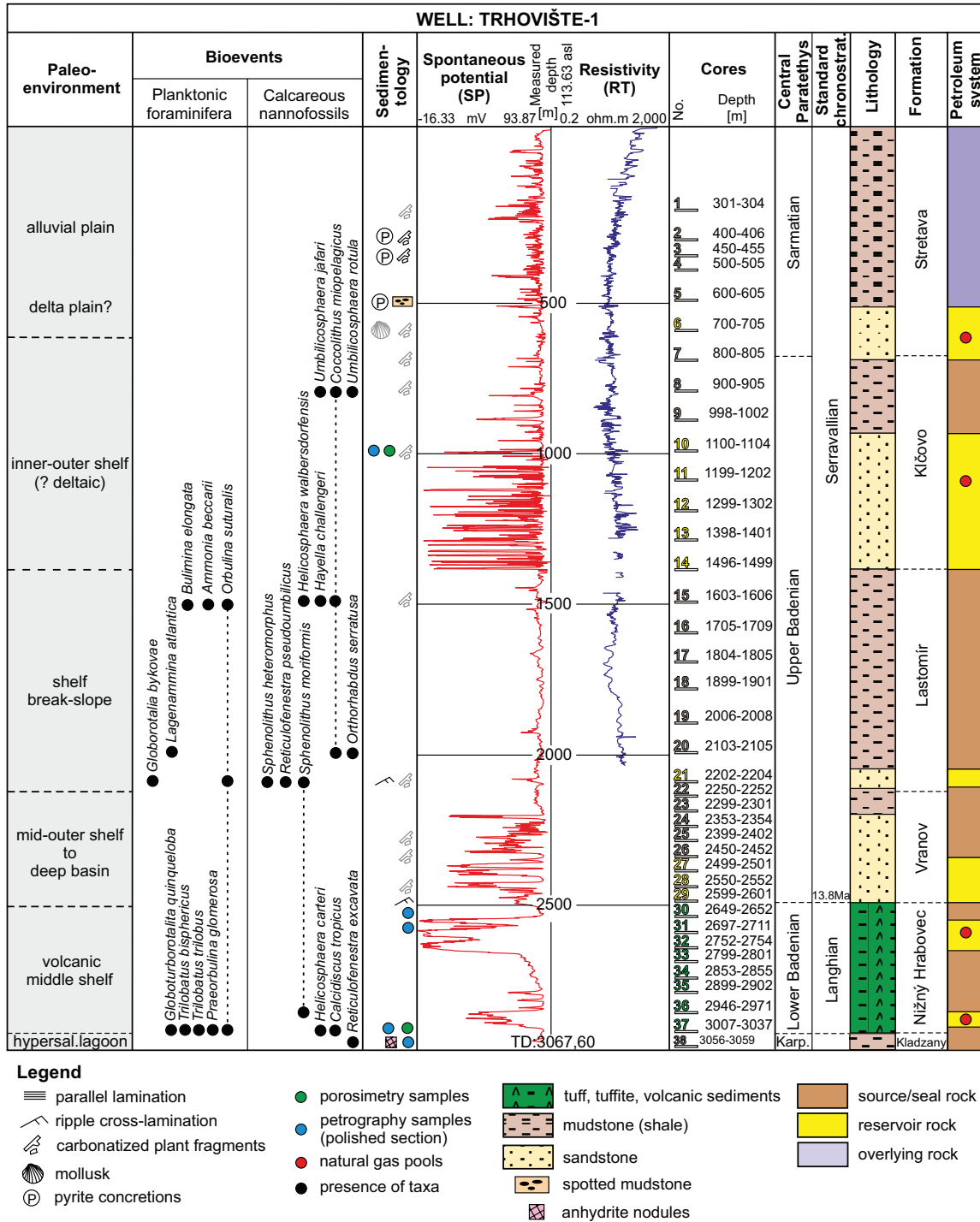**Fig. 12.** Sedimentary profile of the Vranov nad Topľou section.

Fig. 13. Table of the Trhovište-1 well including lithology, formations, age classification (standard chronostratigraphy and Central Paratethys stratigraphy), the position of cores with depth, well-logs (SP and RT logs), sedimentary structures, bioevents (planktic foraminifera and calcareous nannofossils) and paleo-environments. Grey colour marks data explored from the original well-report (Rudinec 1960).

between 3253 and 2895 m (Suppl. S6): ?*Calcidiscus* spp. (core-51, box-1), *Umbilicosphaera jafari, Helicosphaera mediterranea* (core-50, box-2)*, ?Coccolithus miopelagicus* (core-49, box-1)*, Umbilicosphaera jafari, ?Syracosphaera* spp., *Pontosphaera mulripora* (core-45, box-1) and *Coccolithus pelagicus* (core-44, box-1).

Interpretations

Kladzany Formation

An interpretation of the Kladzany Fm. was only gained from the Trhovište-1 well data. From the sedimentological point of

view, the massive calcareous mudstone layers with white anhydrite nodules (TRH-1; 3059–3056 m; core-38) can be connected with a deposition from suspension (Fs) connected with an inner shelf to hypersaline lagoon environment. The nodules point to the fact that the mudstones entered the marginal marine evaporite environment soon after deposition.

From the petrographic perspective, anhydrite nodules (TRH-1; core-38) may provide evidence for the Kladzany Fm., which according to Vass (2002) should yield abundant evaporite concretions. Based on the presence of evaporites, this interval may have formed in an inner shelf, hypersaline lagoon to coastal plain (sabkha). However, evaporites can also be present in the Nižný Hrabovec Fm. (Vass 2002) and thus, assignment of these sediments to this formation, cannot be excluded.

Nižný Hrabovec Formation

With respect to the basic well logs (SP and RT) of STR-1 and TRH-1 well were interpreted as follows. In the interval of 3320–3103 m (STR-1; core-52 to 48), pronounced negative excursions especially in the core-49 (STR-1; 3151–3153 m) can be connected with coarse-grained layers saturated with fluids and/or gas (Rider & Kennedy 2011). The lowest deflections on the SP log may be associated with massive mudstones (STR-1; core-48). In the interval between ~3037–2649 m (TRH-1; core-37 to 30) and 3060–3004 m (STR-1; core-47 and 46) commonly includes higher excursions on the SP log, which is typical for layers of coarse-grained sediments (e.g., lapilli tuffs and volcanic sandstones) and/or rocks saturated by fluids or gas (Rider & Kennedy 2011). On the RT log, low amplitudes indicate high conductivity of the sediments (STR-1; core-47 and 46).

From the sedimentological perspective, the deposition starts with coloured conglomerates with soft sediment deformations (Gm; see Table 1 for all following lithofacies code) in the STR-1 well (core-52 to 51; Fig. 17a). They could point to a short interval deposited in fluvial and or ephemeral lake environment with rare marine ingressions (Fs; Rossi et al. 2017). This interval can be labelled as inner shelf. The sedimentation continues with fine- to coarse-grained zeolitized tuff, redeposited tuffs together with mudstones that include clasts of volcanic origin (Ct/Ctr; NHQ, 1.5 m and below; TRH-1, ~3037–2649 m, core-37 to 30; STR-1, 3320–3004 m, core-52 to 46), which can be associated with pyroclastic deposition. Above, the association of massive, laminated and ripple-cross laminated sandstones (Sm, Sl) continues. This interval was most likely deposited from traction carpet, by low amplitude bed-waves and by fully dilute turbulent flow. Thus, they can be interpreted as Ta and Tb intervals of the Bouma sequence (Talling et al. 2012). Based on this, high-density turbidite currents dominated. This claim is supported by the presence of flutes and grooves (Figs. 4d, 5), which are commonly found at the base of the sandstone beds (NHQ, 1.5–11 m; STR-1, 3202–3004 m, core-50 to 46). On the other hand, the rare intervals of massive mudstones (Fm) intercalated by thin ripple-cross laminated sandstones (Sr), are interpreted as Te and Tc intervals of the Bouma sequence, and they could have been deposited by a dilute fully turbulent flow alternating with deposition from gel with network of bonds and should be a part of low-density turbidites (NHQ, 1.5–11m). Nonetheless, alternation of mudstones (Fm) with rippled sandstone (Sr) can also commonly be interpreted as shelf-transition – outer shelf setting. The presence of glauconite grains, as well as fossil shells reinforces the subaqueous environment interpretation. The palaeontological material (*Trilobatus*
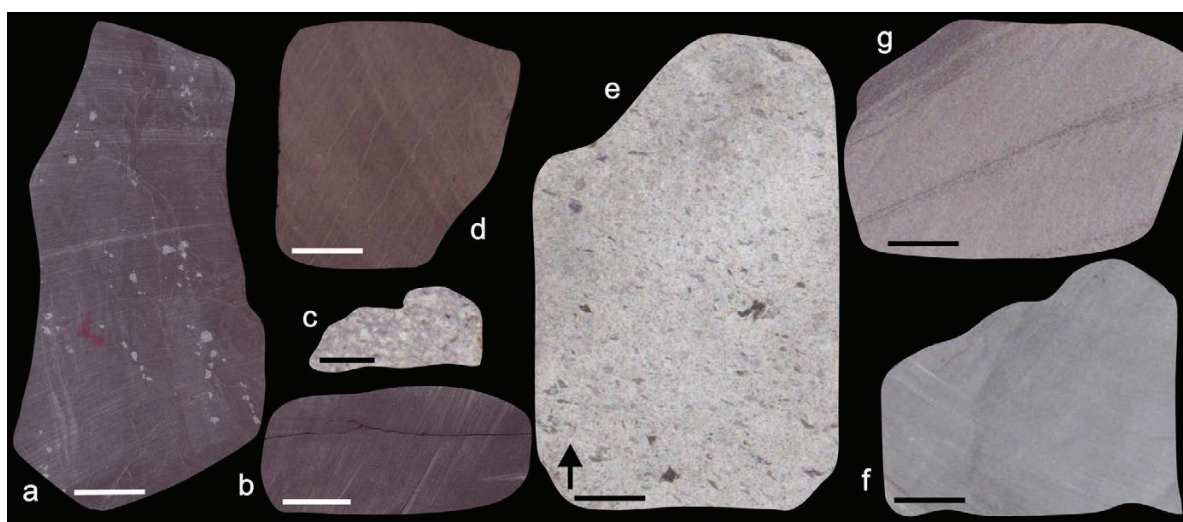

Fig. 14. Well core samples from the Trhovište-1 well. Core = C; Box = B; depth in m, arrow points towards the overburden, black or white line = 1cm. **a** — C38: 3056–3059, B2 – dark brown, massive carbonate mudstones with anhydrite nodules; **b** — C37a: 3007–3012, B2 – dark brown, massive mudstone; **c** — C37: 3007–3012, B2 – grey massive volcanic sediment/tuffite; **d** — C36: 2946–2949, B3 – brown, massive mudstones; **e** — C31: 2698–2711, B4 – grey-green tuffites; **f** — C30: 2649–2652, B3 – grey-green, fine-grained, massive volcanic tuffs/tuffites; **g** — C29: 2599–2601, B2 – grey-brown, massive sandstones.
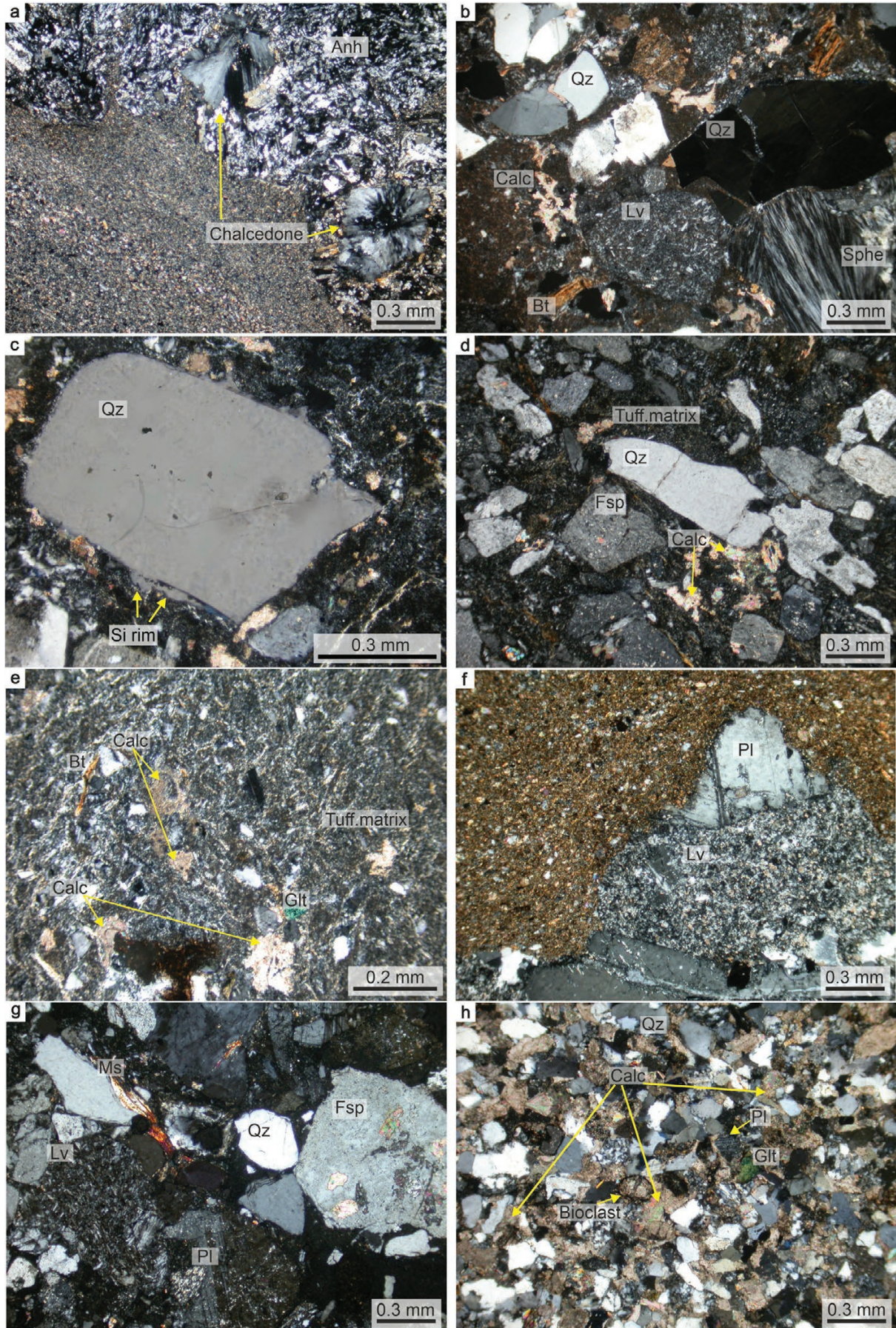
Fig. 15. Thin sections. Core=C; Box=B; depth in m. **TRH-1: a** — C38: 3056–3059, B2 – mudstone with anhydrite (Anh) and chalcedone nodule fill; crossed nicols. For macro see Fig.13a. **b** — C37: 3007–3037, B2 – tuffite composed of quartz (Qz), calcite cement (Calc), biotite (Bt), sphelurite (Sphe) and volcanic lithoclasts (Lv) in tuffitic matrix. Carbonate cement is present; crossed nicols. **c** — C37: 3007–3037 – quartz grain with Si rim in tuffic sandstone. **d** — C31: 2697–2711, B5 – tuffites composed of quartz (Qz), feldspar (Fsp) and calcite cement (Calc) in tuffitic matrix; crossed nicols. **e** — C30: 2649–2652, B3 – tuff/tuffite with biotite (Bt) and glauconite (Glt) in tuffitic matrix and calcite cement (Calc); crossed nicols. **STR-1: f** — C50: 3199–3202 – volcanic lithoclasts (Lv) with porphyric plagioclase (Pl) in clayey-mikritic matrix; crossed nicols. **g** — C47: 3054–3060, B6 – volcanic sediments made up of quartz (Qz), plagioclase (Pl), muscovite (Ms), feldspar (Fsp) and volcanic lithoclasts (Lv); crossed nicols. **h** — C45: 2950–2953 – well sorted sandstone composed of quartz (Qz), plagioclase (Pl), glauconite (Glt) and bioclasts. Calcite and dolomite cement are widespread; crossed nicols.

bisphericus, Praeorbulina curva and *Orbulina universa*) is in favour of these claims and assumes deposition in warm oligotrophic marine conditions (Spezzaferri 1994; Bijma et al. 1990). Moreover, the absence of benthic taxa may point to unfavourable conditions on the seabed, what could have indeed been caused by reoccurring sediment density flows (NHQ, 1.5–11m; STR-1, 3202–3004 m, core-50 to 46). White discontinuous lenticular layers consisted of microsparite (recrystallized from micrite) indicate diagenetic origin. The precursor was most likely calcareous nannoplankton identified from smear slides under an optical microscope. Since it is abundant in these layers, the carbonate accumulation is still probably primary, which is supported by the fact that these layers stick to the bedding planes. Thus, this layer can be interpreted as thin chalk layers affected by diagenesis (NHQ, 6.8–10m; Suppl. S3). Overall, if the classification of Pellegrini et al. (2020) is considered, the interval controlled by turbidites can be associated with the mid – outer continental shelf/plateau to deep basin.

The presence of glauconite, rare bioclasts, and nannoplankton in the studied samples gives evidence of deposition in subaqueous, marine conditions. Moreover, the presence of Fe-chlorite cement (Suppl. S1b; STR-1, 3320–3004 m, core-52 to 46) is typical for a marine environment (Worden et al. 2020). Volcanic lithoclasts of magmatically corroded quartz, fragments of spherulites and oligoclase point to rhyolite volcanism (Fig. 15b). Meanwhile, other detrital grains suggest meta-

morphic- (gneiss, schist) and sedimentary sources (TRH-1, 3012–3007 m; core-37; STR-1, 3320–3004 m, core-52 to 46).

The cement composition from the Nižný Hrabovec Fm. interval of the TRH-1 well was described as follows: Decomposition of rhyolite glasses can be the main source of Si, which led to the formation of silica (Qz) cement. Moreover, uneven quartz overgrowth cement is present in some sides of detrital quartz grains (Fig. 15c). On the other hand, plagioclase grains are overgrown by albite rims. Idiomorphic crystals of authigenic albites together with calcite cement are mainly focused on the remaining intergranular pore space, which indicates their crystallization after the Si cement formation (similar features can be seen in Fig. 6e, f of the Stretava-1 well). For the source of the carbonate cement, the albitization of detrital plagioclase, where Ca is a by-product, was reported by several studies (e.g., Boles 1982; Morad et al. 1989; Hövelmann et al. 2010; Norberg et al. 2011). Generally, the albitization process causes an increase in secondary intragranular porosity (Fig. 6e). However, these newly formed voids in clasts are subsequently filled with carbonate cement or albite. Albite rims around clasts have no visible porosity. The total porosity (6.41 %; core-37; Table 3) can be classified as poor (Koesoemadinata 1980; Suppl. S2). Based on petrographic observation, overgrowths and pore-filling cements may be responsible for this decreased value. Based on this data, the reservoir rock potential of these sediments is low (after Khanin 1965). However, the permeability was not measured.

Table 3: Total porosity and permeability measurements by Unichema Ltd. and data derived from Stretava-1 well report (Rudinec 1965).

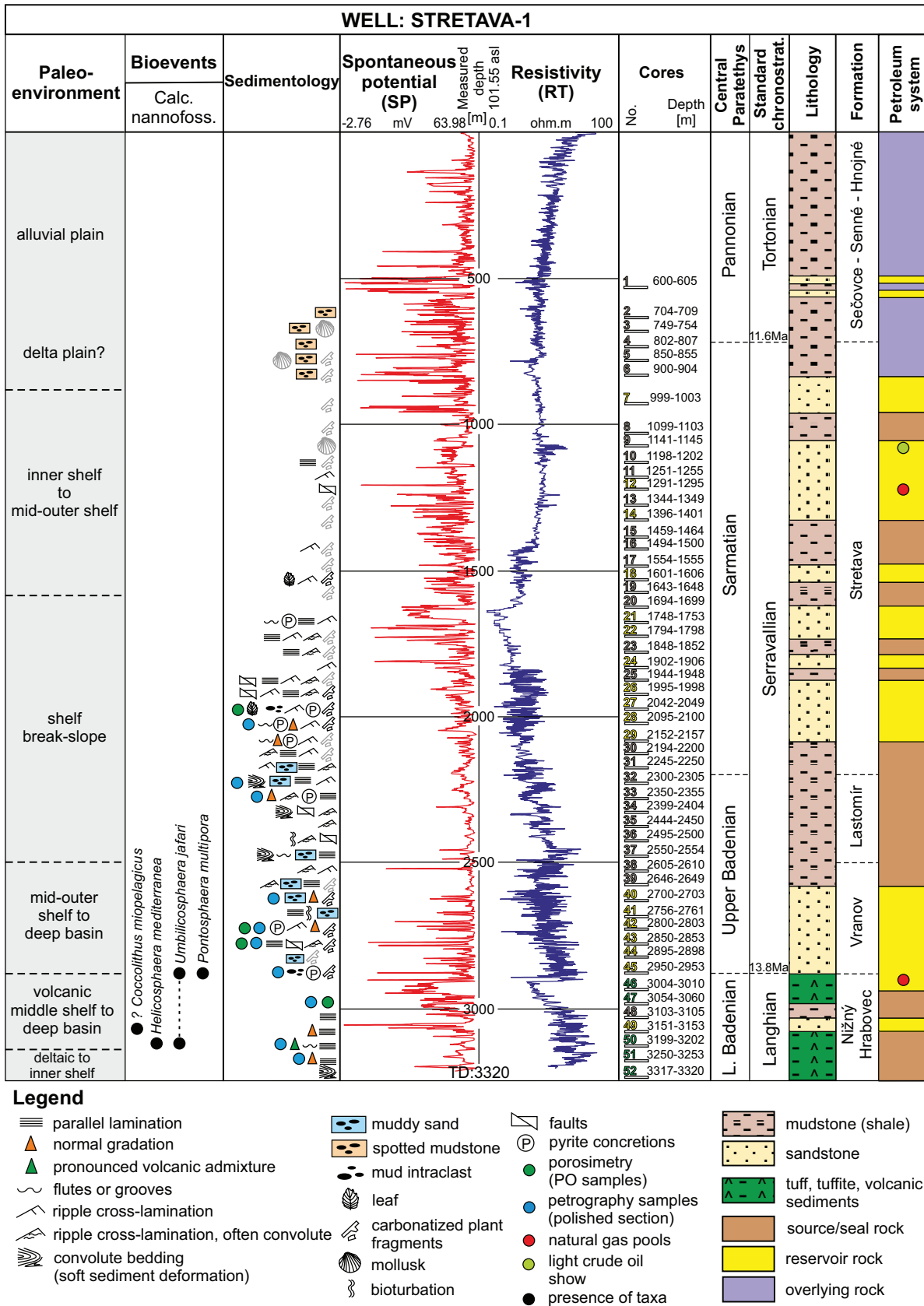| Well/ section	Depth [m]	Core	Porosity		Permeability		Sample gravity	Rock gravity	Specific surface
			total [%]	effective [%]	gas [md]	water [md]	[g/cm³]	[g/cm³]	[m²/g]
original data of this work:									
TRH-1	1100–1104	10	24.09				1.975	2.602	1.186
TRH-1	3007–3012	37	6.41				2.423	2.589	2.447
STR-1	2042–2049	27	13.64		0.155	0.002	2.275	2.634	2.713
STR-1	2800–2803	42	8.85		0.144	0.016	2.422	2.657	0.875
STR-1	2850–2853	43	15.49	6.23	1.780	0.28	2.246	2.658	1.047
STR-1	3054–3060	47	9.95		0.120	0.037	2.388	2.652	0.967
STR-1	3054–3060	47	9.96				2.357	2.618	2.076
NHQ	10		13.21				2.177	2.508	3.783
data derived from petrophysical well report:									
STR-1	3004–3010	46		6–17.8	6.1–9.3				
STR-1	3054–3060	47		11–32.2	6.1–20.2				
STR-1	3151–3153	49	2.7–5.4						

Fig. 16. Table of the Stretava-1 well including lithology, formations, age classification (standard chronostratigraphy and Central Paratethys stratigraphy), the position of cores with depth, well-logs (SP and RT logs), sedimentary structures, bioevents (planktic foraminifera and calcareous nannofossils) and paleo-environments. Grey colour marks data explored from the original well-report (Rudinec 1965).
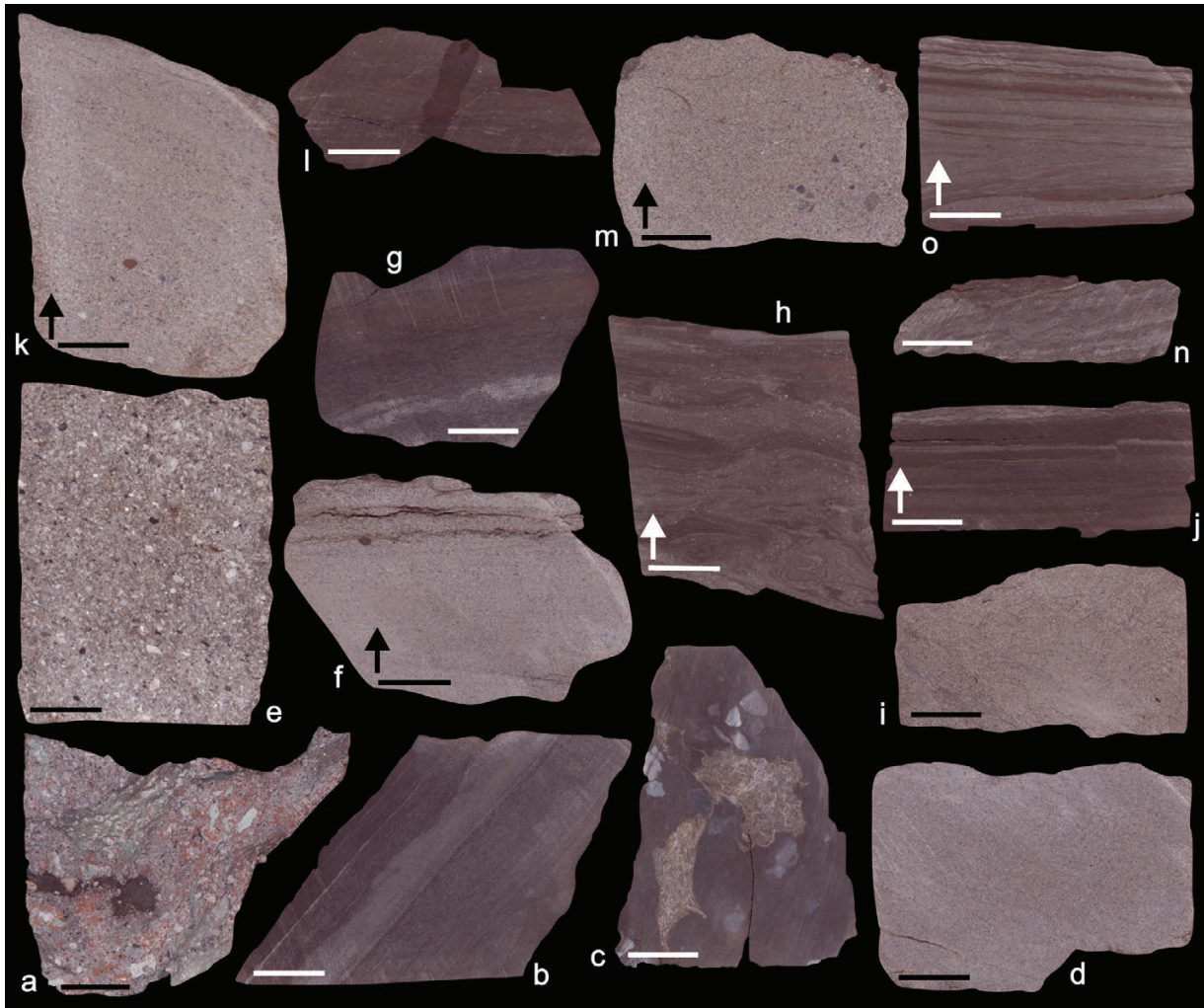
Fig. 17. Well core samples from the Stretava-1 well. Core=C; Box=B; depth in m, arrow points towards the overburden, black or white line=1cm. **a** — C52: 3317–3320, B2 – volcanic, green-grey-red coloured conglomerates, deformed and altered; **b** — C50: 3199–3202, B3 – dark brown, massive mudstones and sandstone with flutes or grooves; **c** — C50: 3199–3202, B1 – dark brown paraconglomerate with volcanic clasts; **d** — C49: 3151–3153, B1 – light brown-grey, fine-grained, massive to graded sandstones; **e** — C47: 3054–3060, B6 – grey, coarse-grained, massive volcanic conglomerate; **f** — C45: 2950–2953, B2 – grey, massive sandstones with mud intraclasts and carbonatized plant fragments; **g** — C45: 2950–2953, B1 – alteration of massive mudstones with sandy convolute ripple-cross laminations; **h** — C44: 2895–2898, B2 – brown, massive sandstones with clay admixture and convolute bedding; **i** — C43: 2850–2853, B4 – light brown, massive sandstones with carbonatized plant fragments; **j** — C43: 2850–2853, B2 – dark brown, laminated to convolute, ripple-cross laminated mudstones, deformed by normal faults; **k** — C42: 2800–2803, B2 – grey, massive to graded sandstones with carbonatized plant fragments; **l** — C41: 2756–2761, B2 – dark brown, massive mudstones with bioturbation; **m** — C40: 2700–2703, B1 – grey, graded sandstones; **n** — C39: 2646–2649, B1 – dark brown, massive mudstones and grey, convolute, ripple-cross laminated sandstones; **o** — C38: 2604–2610, B4 – dark brown, laminated mudstones and ripple-cross laminated sandstones.

The composition of cement of the STR-1 well from the Nižný Hrabovec Fm. interval is more variable than in the TRH-1 well (Nižný Hrabovec Fm.). Although the quartz (?) cement is still predominant, it commonly mixes with illite. The decomposition of volcanic glass can still be considered as the source of Si. For the formation of the authigenic illite, two models were proposed. Either K-fluids need to be present (potassium source) or illite can form from sedimentary precursor minerals. The presence of K-fluids is supported by a small amount of authigenic K-feldspar and may be linked with K-fluids described in zeolites and overlying sandstones (Tschegg et al. 2020; this study). According to Lee & Parsons (2003), K-feldspar formation is a common process just like albitization. Chlorite, calcite, and albite crystals form during the final stage of the paragenetic sequence as pore-filling minerals. A possible source of chlorite cement could be the volcanic clasts (Worden et al. 2020). Pore-filling chlorites induce the reduction of pore-throats, and thus decrease the porosity and permeability (Grigsby 2001; Worden et al. 2020; Zhou et al. 2020). Moreover, calcite often fills the intragranular pores in altered plagioclase. Despite the above-mentioned arguments, the total porosity reached a value of 9.96 %

(core-47; Table 3), which is a higher value than the slightly altered sample from the Trhovište-1 well. Nevertheless, the porosity was classified as poor (after Koesoemadinata 1980) or reduced (after Khanin 1965; Suppl. S2). The measured gas permeability shows a value 0.12 mD. Consequently, according to Koesoemadinata (1980) the reservoir can be classified as tight (3054–3060 m, core-47; Table 3; Suppl. S2).

The cement in the NHQ section differs from cement described in the TRH-1 and STR-1 well (Nižný Hrabovec Fm. interval). According to Tschegg et al. (2019), from the diagenetic point of view, zeolite groundmass is composed of ultrafine crystallites of authigenic cristobalite. The source of siliceous cement is explained as a product of excess Si caused by glass shards zeolitization (Tschegg et al. 2019). In the overlying sandstones siliceous cement is also abundant, and its crystalline form is well documented especially around empty pore spaces (Fig. 6b, d). Admixture of Al, Fe, Ca and K in the cement analyses (Suppl. S1c) point to a presence of a few tiny clay crystals below the probe resolution. The expected source of siliceous cement is zeolites. Similarly, the source of authigenic K-feldspars in zeolites was originally linked with the migration of K-rich fluids along the fault surfaces, where crystallization of K-feldspars in foliation, fractures, and open cavities took place (Tschegg et al. 2020). However, in this study, the authigenic K-feldspar in zeolites was observed outside fault zones (Fig. 6a), which suggest that these fluids were not strictly related to them. Furthermore, the formation of authigenic K-feldspar and overgrowth around detrital K-feldspar (Fig. 6c), was also observed in overlying sediments. The presence of authigenic K-feldspar, and siliceous cement in sandstones supports this claim. The authigenic origin of K-feldspar is supported by the high amount of orthoclase molecule ($Or_{99.34-99.98}$; Fig. 8). The formation of K-feldspar, zeolites, opal and clay minerals by glass transformation is common (e.g., Stamatakis 1989). If very short transport is considered, it cannot be strictly excluded that idiomorphic K-feldspars in sandstones originated from underlying zeolites. The formation of siliceous cement may be responsible for the fair total porosity (PO-1; Fig. 5) with a value of 13.21 % (classification after Koesoemadinata 1980; Table 3; Suppl. S2).

The composition of the planktic association in the Nižný Hrabovec Fm. interval of the TRH-1, STR-1 wells and NHQ section is comparable. In the NHQ section the occurrence of *Trilobatus bisphericus, Praeorbulina curva* and *Orbulina universa* indicate a time range of 16.38 to 14.24 Ma (Figs. 5, 9; Suppl. S3). This is in accordance with the biostratigraphic results of Vass (2002). The presence of *Coccolithus miopelagicus, Reticulofenestra pseudoumbilicus, Discoaster variabilis, Helicosphaera mediterranea* and *Coccolithus pelagicus* together with LO (last occurrence) of *Sphenolithus heteromorphus* most probably point to an age of 13.53 Ma or older (Fig. 10; Suppl. S3). In the TRH-1 well (Nižný Hrabovec Fm.), the interval between 3037 and 2652 m (core-37 to 30; Table 4; Suppl. S5) includes the association of *Praeorbulina glomerosa* (core-37; FO: 15.1 Ma, in the Langhian stage; Aziz et al. 2008), *Orbulina suturalis* (core-37; FO: 14.6 Ma; Aziz et

al. 2008), *Trilobatus bisphericus* (core-37; redeposited from the Karpatian stage; Hohenegger et al. 2014). The association in the STR-1 well (Nižný Hrabovec Fm.) contains a poor calcareous nannofossil assemblage in the interval between ~3320 and 3004 m (core-52 to 46; Suppl. S6): ?*Calcidiscus* spp. (core-51, box-1), *Umbilicosphaera jafari, Helicosphaera mediterranea* (core-50, box-2), ?*Coccolithus miopelagicus* (core-49, box-1), *Umbilicosphaera jafari*, ?*Syracosphaera* spp. (Table 5). All associations from the mentioned intervals (NHQ, TRH-1, STR-1) point to the lower Badenian (Langhian) age.

Vranov Formation

In the interval 2649–2299 m (TRH-1, 2601–2299 m, core-29 to 23; STR-1, 2953–2605 m, core-45 to 38), high amplitude deflections on the SP and RT log indicate the presence of sandstone bodies. They are represented by cylindrical and symmetrical trends, which can be interpreted as gravity sediments (Emery & Myers 1996). Mudstone intercalations are revealed by low excursions on the SP log.

Based on the absence of volcanic material (Vass 2002), this interval can be associated with the Vranov Fm. (VNT section, 0–3.8 m; TRH-1, 2601–2250 m, core-29 to 22; STR-1, 2953–2605 m, core-45 to 38). The massive sandstones (Sm; see Table 1 for all following lithofacies code) and graded to parallel laminated sandstones were probably deposited from traction carpet and by low amplitude bed-waves. This interval is interpreted as Ta and Tb of the Bouma sequence (Fig. 12; Talling et al. 2012). Thin ripple-cross and convolute ripple-cross laminated sandstones (Sr) intercalated by massive mudstones (Fm) are interpreted as Tc and Te intervals of the Bouma sequence. They were likely deposited by a fully dilute turbulent flow alternating with deposition from gel with network of bonds. The above mentioned association may indicate the influence of high-density turbidites overlain by low-density

Table 4: Lithostratigraphy of the Trhovište-1 well.

Depth [m]	Core	Formation	Age
3056–3059	38	Kladzany	Karpatian
3037–2649	37–30	Nižný Hrabovec	lower Badenian
2601–2250	29–22	Vranov	upper Badenian
2204–1603	21–15	Lastomír	upper Badenian
1499–800	14–7	Klčovo	upper Badenian
705–0	6–0	Stretava	Sarmatian

Table 5: Lithostratigraphy of the Stretava-1 well.

Depth [m]	Core	Formation	Age
3320–3004	52–46	Nižný Hrabovec	lower Badenian
2953–2605	45–38	Vranov	upper Badenian
2554–2300	37–32	Lastomír	upper Badenian
2250–802	31–4	Stretava	Sarmatian
754–0	3–0	Sečovce–Senné–Hnojné	Pannonian

turbidite currents and mud. Presence of rare bioturbation points to oxic condition on the seabed (VNT section, 0–1.7 m; TRH-1, 2601–2250 m, core-29 to 22; STR-1, 2953–2950 m, core-45). According to Pellegrini et al. (2020) such an environment could be interpreted as mid-outer shelf to deep basin. Nevertheless, a less probable interpretation of the alternations of the massive mudstones (Fm) and ripple-cross laminated sandstones (Sr) may be linked with heterolithic sedimentation by tidal currents (lenticular, wavy and flaser bedding; Rossi et al. 2017) or other depositional environments. At the height of 80 cm in the VNT section, Te interval is terminated by a discontinuity interpreted as a slump body. It also cannot be excluded that this deformation is related to much later movements of the weathered rocks close to the surface.

In the VNT section, porosity was not measured due to the high degree of alteration and telogenesis (hematite and calcite cement), which was visible in micro- and meso-scale (red colour of sandstones; Fig. 7c, d). Evidence for the secondary cement was also found in the washed residue, which commonly included Fe-oxides. Well rounded, subangular grains in the STR-1 well (Vranov Fm. interval, 2953–2605 m, core-45 to 38) indicate short transport from the source area and reworking. Rare clasts of volcanic origin are accompanied by carbonate and phyllites clasts. High amounts of carbonate cement and/or compaction in thin section samples (core-45) may cause a decrease in porosity.

Based on the obtained taxa in VNT section (Figs. 9, 12, VNT-1, 2, 3, 4; Suppl. S4): *Orbulina suturalis, Globigerina druryi, Globigerina ciperoensis, Globorotalia bykovae, Valvulineria complanata*, *Melonis pompilioides, Bulimina elongate, Bolivina* sp., *Uvigerina grilli, Ammonia parkinsoniana, Elphidium macellum, Textularia gramen, Bogdanowiczia pocutica* and *Rhizammina algaeformis* together with *Sphenolithus heteromorphus, Coronocyclus nitescens* (elliptical)*, Discoaster exilis, Helicosphaera wallichii* (16.38 to 12.6 Ma; Aziz et al. 2008; Gradstein et al. 2020), together with taxa recognized in the STR-1 well (2953–2605 m, core-45 to 38): *Pontosphaera multipora* (core-45, box-1) and *Coccolithus pelagicus* (core-44, box-1) may point to the upper Badenian stage. The outlined stratigraphy was further supported by seismic interpretation of the Composite-1 line (Fig. 18). After the counting of individual specimens it can be stated that the foraminifera index is mixed (*Ammonia–Elphidium* index; AEI – Na/(Na+Ne)*100) and reaches a value of 68.2, which indicates a decreased amount of oxygen on the seabed (Gupta & Platon 2006). Foraminifera species, which do not tolerate decreased oxygen values like Cibicedes–Cibicidoides and keeled Elphidids, may be redeposited into the association.

Seismic interpretation

This chapter includes seismic interpretations of the Trebišov sub-basin, especially around the STR-1 and TRH-1 wells (Figs. 18, 19). Interpretations were made by using the Composite-1 section derived from 3D reflection seismic grid.

Structural interpretation

The most pronounced structures in the deep part of the basin (3000 ms-TWT; Suppl. S7) have a NW to SE trend and dip in a 45° angle towards the SW. The less evident structures have a N to S trend and dip towards the E to NE (Suppl. S7). The structures can be interpreted as Riedel and P-shears developing in a strike-slip fault zone (Naylor et al. 1986). In the depth of 2000 ms-TWT (Suppl. S7), a main fault (trending: NW to SE; dip: SW) can be clearly recognized, and it begins around the Trhovište area and continues towards the SE to the Stretava area. This fault is further associated with multiple extensional fractures with low angles to the main fault (trending: N to S; dip: W). These structures may be interpreted as splay faults (Naylor 1986). The main fault, and the associated splay faults are even better visible in the depth of 1000 ms-TWT (Suppl. S7). Moreover, the master fault can be indistinctly recognized south of the main fault and joins the main fault by means of its associated splay faults (around the Trhovište area). The trend of the master fault is similar to the main fault, but it has a NE dip (30 to 40° angle). The described structures can be interpreted as two opposing horsetail structures. An indistinct detachment seems to be present between the sediments of the Central Carpathian Paleogene Basins (CKP) and the lower Miocene sediments (Figs. 18, 19). Presence of downlaps at the Karpatian and lower Badenian boundary indicates a period of non-deposition. Consequently, the Trebišov sub-basin can be interpreted as a typical interplate pull-apart basin et least during the lower Miocene time (Allen & Allen 2013). Thus, it can relate to the first syn-rift stage of the basin. Within the lower and upper Badenian stage the thickening towards the master faults is indistinct. Nevertheless, during the Sarmatian stage the master fault seems to be reactivated and the sediments are growing towards it again. This process may relate to a continental back-arc basin development (Allen & Allen 2013), and thus to the second syn-rift stage of the basin. The Pannonian interval is deformed only very slightly, which could be associated with differential compaction and consequently this time interval may point to onset of the post-rift thermal subsidence (Figs. 18, 19; Suppl. S7).

Seismic sequence (Sse) and facies (Sf) interpretation

Sse1: The Karpatian (Kladzany Fm. 1-2; Fig. 20) seismic sequence is defined by baselaps on the lower boundary and by concordance at the upper boundary. The seismic sequence is split into 2 seismic facies (Sf1-2). **Sf1:** The facies seem to be parallel to sub-parallel with continuous to discontinuous reflections. Amplitudes are low to very low with medium frequencies. Lithology of the facies is mudstone dominated. The depositional environment is interpreted as inner shelf, hypersaline lagoon to coastal plain (sabkha). **Sf2:** The seismic reflection configuration is sub-parallel and arranged in sigmoid to oblique prograding clinoform. The reflections are mostly discontinuous with very high to high amplitude and broad frequencies. The facies are composed of coarse-grained
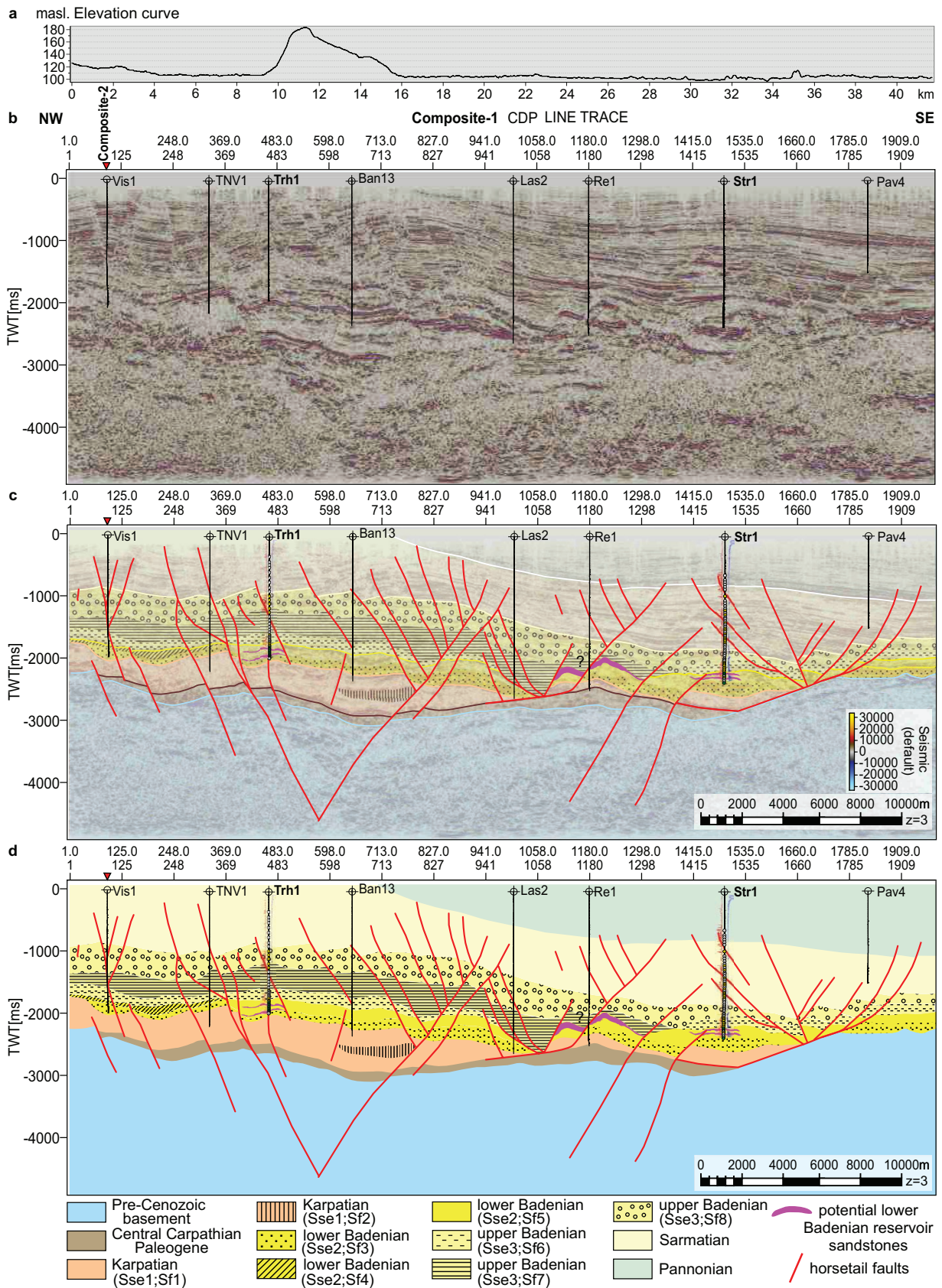
Fig. 18. Composite-1 reflection seismic line (extracted from 3D grid): **a** — Digital elevation model cross-section; **b** — Clean seismic line with projected wells; **c** — Seismic line with highlighted faults, projected wells and interpreted seismic facies together with lower Badenian reservoir sandstone bodies (in pink); **d** — Interpreted line with highlighted tectonic structures and sedimentary facies.
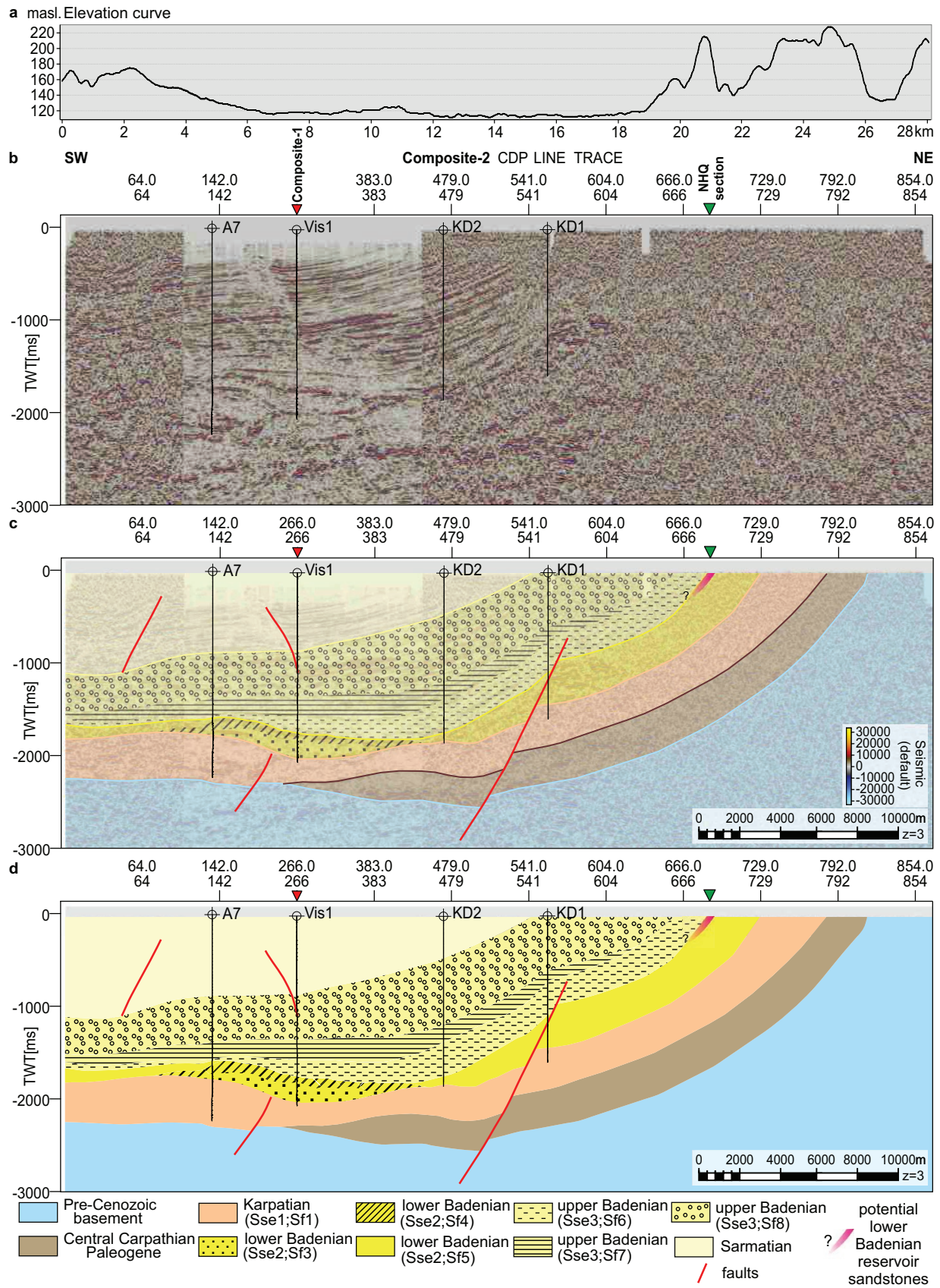
Fig. 19. Composite-2 reflection seismic line (extracted from 2D and 3D grid): **a** — Digital elevation model cross-section; **b** — Clean seismic line with projected wells; **c** — Seismic line with highlighted faults, projected wells and interpreted seismic facies together with lower Badenian reservoir sandstone bodies (in pink); **d** — Interpreted line with highlighted tectonic structures and sedimentary facies.

and/or volcanoclastic sediments. The paleo-environment can be associated with coarse-grained delta.

Sse2: The lower Badenian (Nižný Hrabovec Fm. 1–3; Fig. 20) seismic sequence evinces baselaps on the lower boundary and concordance on the upper boundary. The seismic sequence is divided into 3 seismic facies (Sf3–5). **Sf3:** The seismic reflections are parallel and continuous with very high amplitudes. Frequency is medium to broad. The lithological fill is represented by green-grey-red coloured volcanic conglomerates with soft sediment deformation, which points to the fluvial dominated setting (Rossi et al. 2017) and inner shelf environment. **Sf4:** The seismic facies display sub-parallel sigmoid to oblique prograding clinoform with continuous reflections in the upper part and discontinuous in the middle and lower part. Facies show high to low amplitude with narrow to medium frequency. Due to the individual clinotheme dip ~12.5°, the lithology can be interpreted as sandy (Pellegrini et al. 2020). Thus, the seismic facies were most likely accumulated in the mid-shelf / prodelta slope environment (Pellegrini et al. 2020). **Sf5:** The seismic facies evince parallel, mostly continuous, occasionally discontinuous reflections with high to medium amplitude. Frequency can be classified as narrow to medium. Sediments in the given interval include fine-grained massive to rhythmic laminated sandstones intercalated by mudstones. This deposition can be interpreted as

sedimentation by high-density turbidite currents in mid-outer shelf to deep basin environment.

Sse3: The upper Badenian (Vranov Fm., Lastomír Fm. and Klčovo Fm.; Fig. 21) seismic sequence limited by downlaps on the lower boundary and by concordance on the upper boundary. It was possible to distinguish 3 seismic facies (Sf6–8). **Sf6:** The reflection configuration of the Vranov Fm. is parallel to sub-parallel, and the reflections are continuous to discontinuous. Amplitudes are very high at the top and low at the base. Frequency is medium, occasionally broad. Sediments contain mainly sandstones intercalated by mudstones. The depositional environment was connected with shelf break-slope to deep basin controlled by high-density turbidites overlain by low-density turbidites and mud. **Sf7:** The reflections of the Lastomír Fm. are sub-parallel and predominantly discontinuous. Amplitudes are primarily low with variable frequencies. Lithology is mudstone dominated and deposition took place from suspension in shelf break-slope environment. **Sf8:** The seismic reflections of the Klčovo Fm. are mostly parallel and continuous with high to medium amplitudes. The frequencies are medium. The formation is sandstone dominated and intercalated by mudstones. The environment of deposition is connected to inner-outer shelf (? deltaic).

Other seismic sequences and facies are not discussed as they are not connected with the main aims of this work.
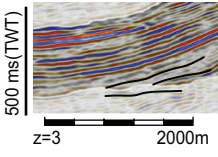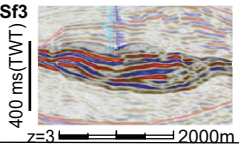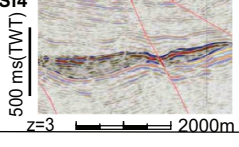

Fig. 20. Seismic sequence, seismic facies and lithostratigraphy description of Karpatian and lower Badenian strata (Sse1, Sf1-2; Sse2, Sf3-5).
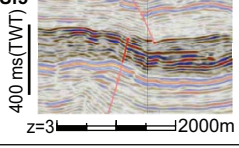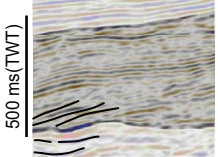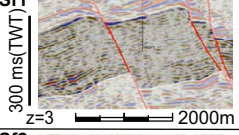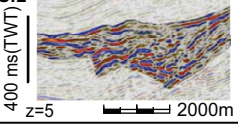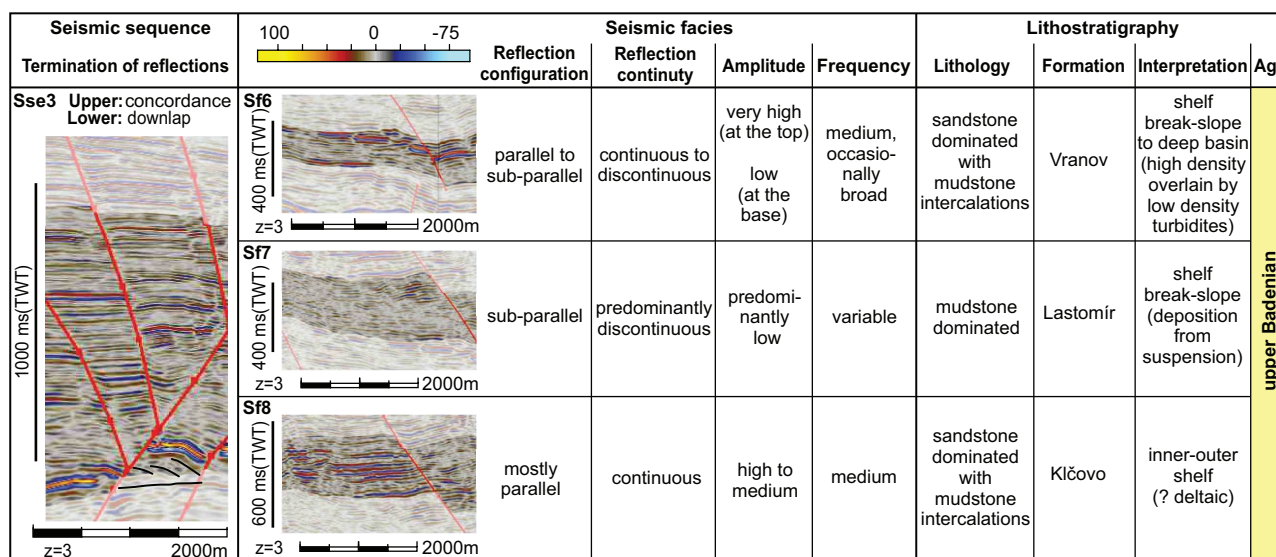
Seismic sequence	Seismic facies					Lithostratigraphy			
Termination of reflections	Reflection configuration	Reflection continuty	Amplitude	Frequency		Lithology	Formation	Interpretation	Age
Sse3 Upper: concordance Lower: downlap	**Sf6** parallel to sub-parallel	continuous to discontinuous	very high (at the top) low (at the base)	medium, occasionally broad		sandstone dominated with mudstone intercalations	Vranov	shelf break-slope to deep basin (high density overlain by low density turbidites)	upper Badenian
	Sf7 sub-parallel	predominantly discontinuous	predominantly low	variable		mudstone dominated	Lastomír	shelf break-slope (deposition from suspension)	
	Sf8 mostly parallel	continuous	high to medium	medium		sandstone dominated with mudstone intercalations	Klčovo	inner-outer shelf (? deltaic)	

Fig. 21. Seismic sequence, seismic facies and lithostratigraphy description of upper Badenian strata (Sse3, Sf6-8).

Discussion

Lower Badenian depositional environments

Although the Nižný Hrabovec Formation was originally assigned to the lower Badenian and the Vranov Formation was to the middle Badenian stage (following the three-fold subdivision of the Badenian stage; Vass 2002), this study assigns the Nižný Hrabovec Formation to the lower Badenian and the Vranov Formation to the upper Badenian (Kováč et al. 2007 and 2018), following the subdivision of the Badenian stage into lower and upper substages according to Kováč et al. (2007 and 2018).

According to Kováč (2000), Vass (2002) and Vass et al. (2005), the **Nižný Hrabovec Formation** should include calcareous, volcanic sandstones, mudstones, and layers of zeolitized rhyodacite tuffs. This was unambiguously confirmed by the results of this study. Although this work did not find gypsum concretions mentioned by Vass (2002), one sample from the Trhovište-1 well (3056–3059 m) verified presence of anhydrite nodules. Nonetheless, it is unclear if this sample belong to the Nižný Hrabovec Fm. or to the Kladzany Fm., which is also known to include evaporites (Vass & Čverčko 1985). The depositional environment of the Nižný Hrabovec Fm. was interpreted by Kováč & Zlinská (1998) and Vass (2002) as an open marine shelf. Later, Vass et al. (2005), further specified the environment as outer shelf. The sedimentological and palaeontological results of this study reveal that the Nižný Hrabovec Fm. starts with fluvial dominated (Sf3) and deltaic (Sf4) inner shelf facies. In the overburden, the facies change to predominantly high-density turbidites deposited in middle shelf to deep basin (Sf5) environment affected by volcanic activity (Fig. 22a).

The Nižný Hrabovec Formation discordantly overlies the Karpatian (Kladzany Formation), Pre-Neogene basement

(Vass 2002), and occasionally rests on the Inner Carpathian Paleogene Basin (CKP) sediments (this study). The stratotype section of the Nižný Hrabovec Fm. was confirmed in the Trhovište-1 well (2645–3037 m). The thickness of the Nižný Hrabovec Formation in the STR-1 and TRH-1 wells is about 400 metres. In the Nižný Hrabovec quarry, the formation is more than 80 metres thick. The exposure shows 9.5 metres of sandstones and mudstones, and the rest sediments are composed of the zeolitized Hrabovec Tuffs. The individual sandstone layers are 10–40 cm thick, which is within the sandstone thickness range (0.5–300 cm) mentioned by Vass et al. (2005).

The foraminifera associations determined by Cicha & Kheil (1962) consist of *Orbulina suturalis*, praeorbulinas and large lagenides, *Lenticulina calcar, L. cultrata, L. auris.* Kováč and Zlinská (1998) determined *Praeorbulina glomerosa, Orbulina suturalis, Trilobatus quadrilobatus* and *Trilobatus trilobus*. Similar association was also identified in this study. Lehotayova (1982) documented *Sphenolithus heteromorphus*, and the presence of this nannofossil was also confirmed in this work. Consequently, the Nižný Hrabovec Formation belongs to the lower Badenian substage (Figs. 9, 10; Suppl. S3).

Kováč (2000), Vass (2002) and Vass et al. (2005) state that the **Vranov Fm.** should be composed of grey calcareous mudstones and sandstones. In comparison to the Nižný Hrabovec Fm., the Vranov Fm. should not include zeolitized rhyodacite tuffs. The presented study supports these claims. The transition between these two formations is clearly visible in the wells (Figs. 13, 16) and composite section (Fig. 18). Vass (2002) assigned these deposits to a shallow marine shelf environment (Fig. 22b). It is difficult to assess this inference because the sedimentary structures (Sr/Fm) may point to either **1)** tidal currents or to **2)** turbidity currents and several further, distinct depositional processes. Nonetheless, this study leans towards the interpretation of high-density turbidite currents
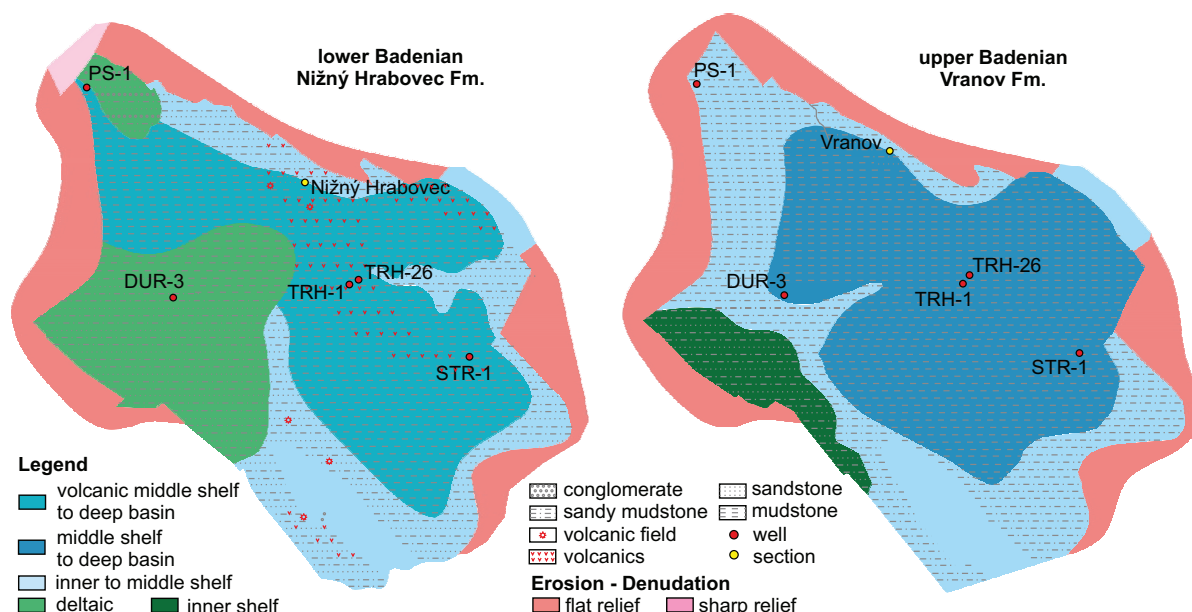
Fig. 22. Interpretation of the depositional environment: **a** — Lower Badenian – Nižný Hrabovec Fm; **b** — Upper Badenian – Vranov Fm. Modified after Vass et al. (2005).

overlain by low-density turbidites and mud. According to Pellegrini et al. (2020), the deposition environment can be specified as mid-outer shelf to deep basin. Alternation of bathyal and littoral fauna in the Zemplínske vrchy Hills (Baňacký et al. 1989; Zlinská 1992a, b) could support redeposition of the littoral fauna into the deep basin, and thus the presence of turbidity currents. The Vranov Fm. may laterally pass into the Zbudza Fm. formed by halite, anhydrite, gypsum and salt clays (Vass 2002). Speculatively, this indicates evaporation on the exposed shelf connected to major sea-level fall, which took place during the Badenian Salinity Crisis 13.81±0.08 Ma and 13.32±0.07 Ma (de Leeuw et al. 2010, 2018; Śliwiński et al. 2012; Šarinová et al. 2021). Consequently, this event dates the boundary between the lower (Nižný Hrabovec Fm.) and upper (Vranov Fm.) Badenian in the basin (~13.8 Ma).

The Vranov Fm. concordantly overlies the Nižný Hrabovec Fm., and the interval is discordantly covered by the Lastomír Formation (Vass 2002). The sediments observed in the partial stratotype section were also recognized in the TRH-1 well, which is the original stratotype (2221–2645 m). The thickness of the Vranov Fm. in the TRH-1 and STR-1 wells reaches about 350 metres.

The foraminifera associations determined by Baňacký et al. (1989) and Zlinská (1996) consisted of *Spiroplectammina carinata, Valvulineria arcuata, V. marmaroschensis, Bulimina elongata, Uvigerina* aff. *rugosa*, *Uvigerina pygmoides, U. aculecta, U. hispida, U.* aff. *asperula* and *U.* aff. *Costata* and a similar association was also identified by this study. The agglutinated species together with a high abundance of *Helicosphaera walbersdorfensis* point to the redeposition of the NN5 into the NN6 zone and indicates the late Badenian age of the Vranov Formation (Fig. 10; Suppl. S4).

Reservoir rocks characterization and prediction

The reservoir rocks in the East Slovakian Basin are mainly formed by fine-grained sandstones with clay matrix and by coarse-grained sandstones (Vass et al. 2005). This finding was also confirmed by petrography of the lower Badenian well-core samples from the TRH-1 and STR-1 wells (Figs. 13, 16). The physical properties are variable (Vass et al. 2005), depending on compositional differences between formations driven by distinct depositional processes. Vass et al. (2005) reported that some samples of sandstones were rich in tuffaceous admixture, especially in the Nižný Hrabovec Formation (lower Badenian).

Reed et al. (1993) documented that the porosity of the sediments (from 35 to 0.1 %) in the East Slovakian Basin tends to decrease with depth (Fig. 23). This observation generally correlates with the results revealed by this study, where the total porosity of the lower Badenian sandstones at the surface reaches 13.21 % (the Nižný Hrabovec section) and in the deep wells has a value of 6.41 % (TRH-1; 3007–3012 m) and 9.96 % (STR-1; 3054–3060 m; Table 3). These values are classified as low to reduced (Khanin 1965, 1969) or as poor (Koesoemadinata 1980; Suppl. S2). It is necessary to note that total porosity is always higher than effective porosity (Dandekar 2013). Despite this fact, effective porosity of at least 1 to 4 % can be sufficient for hydrocarbon extraction. For example, these levels were detected in the Ptrukša field (effective porosity: 1 to 28 %; Ptrukša pumping test) and in the Trhovište– Pozdišovce field (effective porosity: 4 to 29 %; Řeřicha & Palšová 2000).

The pore spaces are dominantly filled with silica cement with different degrees of crystallization and original clayey matrix, which was partially transformed to diagenetic clay

mineral (Fig. 6g). The variability in porosity can be caused by addition of other cement generations (pore-filling chlorite, calcite, albite and illite; Fig. 6g, h). This may reflect the changing provenance (admixture of non-volcanic material), and transport mechanism. During albitization, secondary porosity is formed, but this has probably no major influence on porosity increase (Taylor et al. 2015). This process led to the formation of calcite and albite cement, which formed as pore-filling minerals, during the final stage of the paragenetic sequence. Grain-coating chlorite cement (or illite), which hinders grain overgrowths (Grigsby 2001; Worden et al. 2020; Zhou et al. 2020), was not observed in the studied samples. It remains uncertain what portion of the total porosity corresponds to inter-crystalline pores in the cement.

On the other hand, the Sarmatian sandstones from the TRH-1 well (1100–1104 m, Table 3) have very high (Khanin 1965, 1969) or very good porosity (Koesoemadinata 1980; Suppl. S2), which reaches a value of 24.09 %.

During the deposition of the Nižný Hrabovec Formation, the coarse-grained material entered the basin from the NE and propagated into the basin towards the SW (Vass et al. 2000). In the deep segments of the basin, the lower Badenian sandstone bodies are interpreted as deposits of high-density turbidite currents overlain by low-density turbidites and mud. After the deposition of these sandstones, the basin was deformed by strike-slip faults (horsetail; Fig. 18; Suppl. S7) and/or normal faults, which fragmented the sedimentary bodies and allowed for structural trap formation near the TRH-1 and STR-1 wells (Fig. 18). This inference is in accordance with the interpretations of Rudinec (1976).

With regard to the reservoir rock prediction, the strike-slip deformation seems to have produced two anticlinal structures near the Rebrín-1 well (Re-1; Fig. 18). In the upper part of the lower Badenian interval drilled by the Re-1 well (Rudinec 1969), these structures most likely include reservoir sandstone bodies, and thus may be of exploration interest in the future. These bodies seem to be sealed in the NW–SE direction, but their shape, continuation and sealing towards the NE–SW needs to be confirmed by 3D seismic interpretation in the future.

Conclusion

Based on the planktic foraminifera and calcareous nannoplankton zonation, the Badenian stage in the Trebišov subbasin is divided into lower and upper intervals. This work mainly focuses on the lower Badenian strata of the East Slovakian Basin, which includes the Nižný Hrabovec Formation predominantly composed of conglomerates, zeolitized rhyolite tuffs together with volcanic sandstones and mudstones. These sediments were deposited on fluvial dominated inner shelf to mid-shelf/prodelta slope. They are overlain by sediments deposited by predominantly high-density turbidite currents that accumulated in mid-outer shelf to deep basin. The upper Badenian Vranov Formation is made up of
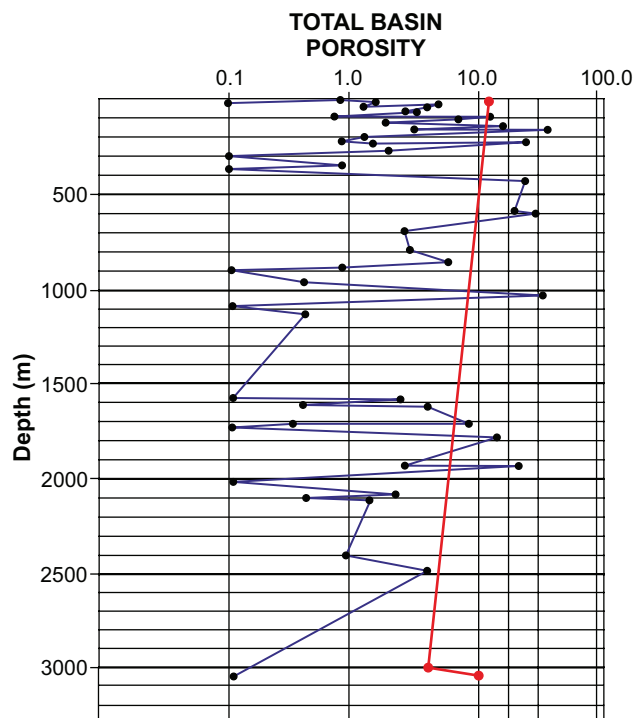

Fig. 23. Porosity vs. depth diagram. Showing sediment porosity from the entire East Slovakian Basin (blue dots; modified after Reed et al. 1993). Plotted against total sandstone porosity acquired by this study (red dots).

calcareous mudstones and sandstones with absence of tuffs and tuffites. The depositional mechanism of this formation can be associated with high-density turbidites overlain by low-density turbidites and mud, which point to the mid-outer shelf to deep basin.

The lower Badenian sandstones were analysed with a focus on their reservoir properties. The presence of glauconite grains, alteration of the tuffs into zeolites, Fe-chlorite cement as well as marine fossils reinforces interpretation that the deposition took place in a marine environment. The total sandstone porosity measurements indicate a gradual porosity decrease with depth marked by a value of 13.21 % at the surface, down to values of 6.41 % at ~3 km below the surface. From the perspective of reservoir potential, the total porosity is classified as low to reduced or poor. The variation of low porosity values can be explained by diagenetic processes such as compaction, silica cementation with various grades of crystallinity, and the formation of other diagenetic minerals such as illite, chlorite and feldspar cement. Advanced grade of albitization was observed in sandstones buried deeper than ~3 km. The potential lower Badenian reservoir sandstones in the vicinity of the studied wells are commonly deformed by strike-slip faults (horsetail structures), and so may frequently form structural traps. Moreover, the lower Badenian sandstones are present at the top of two anticlinal structures near the Rebrín-1 well, with very high reflection amplitudes, and so could be of interest for further exploration.

References

Allen P. & Allen J. 2013: Basin Analysis: Principles and Application to Petroleum Play Assessment. *A John Wiles and Sons*, 1–619.

Aziz A., Stefano A., Foresi L., Hilgen F., Iaccarino S., Kuiper K., Lirer F., Salvatorini G. & Turco E. 2008: Integrated stratigraphy and ⁴⁰Ar/³⁹Ar chronology of early Middle Miocene sediments from DSDP Leg 42A, Site 372 (Western Mediterranean). *Palaeogeography, Palaeoclimatology, Palaeoecology* 257, 123–138. https://doi.org/10.1016/j.palaeo.2007.09.013

Bagdasarjan G.P., Slavik J. & Vass D. 1971: Chronostratigrafický a biostratigrafický vek niektorých významných neovulkanitov východného Slovenska. *Geologické Práce, Správy* 55, 87–96 (in Slovak).

Baňacký V., Eletko M., Kaličiak M., Straka P., Škvarka L., Sucha P., Vass D. , Vozárová A. & Vozár J. 1989: Vysvetlivky ku geologickej mape južnej časti Východoslovenskej nížiny a Zemplínskych vrchov 1:50 000. *The State Geological Institute of Dionýz Štúr*, Bratislava, 1–143 (in Slovak).

Baráth I., Kováč M., Soták J. & Lankreijer A 1997: Tertiary collision, metamorphism and basin forming processes in the Eastern Slovakia (central Western Carpathians). In: Grecula P. et al. (eds.): Geological evolution of the Western Carpathians. *Mineralia Slovaca*, Bratislava, 65–79.

Biela A. 1978: Deep wells in Western Carpathians. *The State Geological Institute of Dionýz Štúr*, Bratislava, 1–224 (in Slovak).

Bijma J., Faber W.W. Jr. & Hemleben C. 1990: Temperature and salinity limits forgrowth and survival of some planktonic foraminifers in laboratory cultures. *Journal of Foraminiferal Research* 20, 95–116.

Boles J. 1982: Active albitization of plagioclase, Gulf Coast Tertiary. *American Journal of Sciences* 282, USA, 165–180.

Boote D., Sachsenhofer R., Tari G. & Arbouille D. 2018: Petroleum provinces of the Paratethyan region. *Journal of Petroleum Geology* 41, 247–298. https://doi.org/10.1111/jpg.12703

Bouma A.H., Normark W.R. & Barnes N.E. 1985: Submarine Fans and Related Turbidite Systems. *Springer Verlag*, New York, 1–351.

Brodňan M., Dobra E., Polášek S., Prokšová D., Račický M., Slávik J. & Sýkorová V. 1959: Geológia Podvihorlatskej uhoľnej panvy, oblasť Hnojné. *Geologické Práce, Správy* 52, 5–69 (in Slovak).

Brown L.F. Jr. & Fisher W.L. 1980: Seismic Stratigraphic Interpretation and Petroleum Exploration. *AAPG Continuing Education Course* 16, 1–56. https://doi.org/10.1306/CE16409

Bown P.R. 1998: Calcareous Nannofossil Biostratigraphy. *British Micropalaeontological Society*, *Publications Series. Chapman & Hall*, London, 1–315.

Cicha I. & Kheil J. 1962: Mikrobiostratigrafie miocénu východoslovenské neogénní oblasti. *Sborník Ústředního ústavu geologického, Oddíl paleontologický* XXVII, 315–348.

Cicha I., Rögl F., Rupp Ch. & Čtyroká J. (Eds.) 1998: Oligocene–Miocene foraminifera of the Central Paratethys. *Abhandlungen der Senckenbergischen Naturforschenden Gesellschaft* 549, 1–325.

Coe A.L. 2003: The Sedimentary Record of Sea-Level Change. *Cambridge University Press*, Cambridge, 1–287. https://doi.org/10.2277/0521831113

Čverčko J., Ďurica D. & Rudinec R. 1969: Příspěvek k hranici torton–sarmat ve východoslovenské neogenní pánvi. In: Zpráva geologického výzkumu v roce 1967. Praha, 252–254 (in Czech).

Dandekar A.Y. 2013: Petroleum reservoir rock and fluid properties (Second edition). *CRC press*, 1–508. https://doi.org/10.1201/b15255

de Leeuw A., Bukowski K., Krijgsman W. & Kuiper K.F. 2010: Age of the Badenian salinity crisis; impact of Miocene climate variability on the circum-Mediterranean region. *Geology* 38, 715–718. https://doi.org/10.1130/G30982.1

de Leeuw A., Tulbure M., Kuiper K.F., Melinte-Dobrinescu M.C., Stoica M. & Krijgsman W. 2018: New ⁴⁰Ar/³⁹Ar, magnetostratigraphic and biostratigraphic constraints on the termination of the Badenian Salinity Crisis: Indications for tectonic improvement of basin interconnectivity in Southern Europe. *Global Planet Change* 169, 1–15. https://doi.org/10.1016/j.gloplacha.2018.07.001

Emery D. & Myers K.J. 1996: Sequences tratigraphy. *Blackwell*, Oxford, 1–297.

Fischer K.C. & Veeken P. 2015: Seismic and Sequence Stratigraphy. *Montan universität*, Leoben, 1–112.

Folk R.L. 1968: Petrology of Sedimentary Rocks. *Hemphill Publishing Company*, Austin, 1–170.

Franců J., Rudinec R. & Šimánek V. 1989: Hydrocarbon generation zone in the East Slovakian Neogene Basin: model and geochemical evidence. *Geologica Carpathica* 40, 355–384.

Franko O., Remšík A., Fendek M., Fusán O. & Zvara I. 1995: Atlas geotermálnej energie Slovenska. *The State Geological Institute of Dionýz Štúr*, Bratislava, 1–164 (in Slovak).

Fusán O., Biely A., Ibrmajer J., Plančár J. & Rozložník L. 1987: Basement of the Tertiary of the Inner West Carpathians. *The State Geological Institute of Dionýz Štúr*, Bratislava, 1–123 (in Slovak).

Gradstein F.M., Ogg J., Schmitz M. & Ogg G. 2020: Geologic Time Scale (1st Edition). *Elsevier*, 1–1390. https://doi.org/10.1016/B978-0-12-824360-2.00001-2

Grigsby J. 2001: Origin and growth mechanism of authigenic chlorite in sandstones of the lower Vicksburg Formation, South Texas. *Journal of Sedimentary Research*, 71, 27–36. https://doi.org/10.1306/060100710027

Gupta B.S. & Platon E. 2006: Tracking past-sedimentary records of oxygen depletion in coastal waters: Use of the Ammonia-Elphidium foraminiferal index. *Journal of Coastal research* 39, 1351–1355.

Hlavatý I., Šály B. & Jureňa V. 2009: Efektívny prieskum uhľovodíkov na Slovensku. *Slovgas*, Bratislava, 13–14 (in Slovak).

Hohenegger J., Ćorić S. & Wagreich M. 2014: Timing of the Middle Miocene Badenian Stage of the Central Paratethys. *Geologica Carpathica* 65, 55–66. https://doi.org/10.2478/geoca-2014-0004

Holbourn A., Kuhnt W., Clemens S., Prell W. & Andersen N. 2013: Middle to late Miocene stepwise climate cooling: Evidence from a high-resolution deep water isotope curve spanning 8 million years. *Paleoceanography* 28, 688–699. https://doi.org/10.1002/2013PA002538

Horváth F., Musitz B., Balázs A., Végh A., Uhrin A., Nádor A., Koroknai B., Pap N., Tóth T. & Wórum G. 2015: Evolution of the Pannonian Basin and its geothermal resources. *Geothermics* 53, 328–352.

Hók J., Šujan M. & Šipka F. 2014: Tectonic division of the Western Carpathians: an overview and a new approach. *Acta Geologica Slovaca* 6, 135–143.

Hövelmann J., Putnis A., Geisler T., Schmidt B. & Golla-Schindler U. 2010: The replacement of plagioclase feldspars by albite: observations from hydrothermal experiments. *Contributions to Mineralogy and Petrology* 159, 43–59. https://doi.org/10.1007/s00410-009-0415-4

Iaccarino S.M., Di Stefano A., Foresi L.M., Turco E., Baldassini N., Cascella A., Da Prato S., Ferraro L., Gennari R., Hilgen F.J., Lirer F., Maniscalco R., Mazzei R., Riforgiato F., Russo B., Sagnotti L., Salvatorini G., Speranza F. & Verducci M. 2011: High-resolution integrated stratigraphy of the upper Burdigalian–lower Langhian in the Mediterranean: the Langhian historical stratotype and new candidate for defining its GSSP. *Stratigraphy* 8, 199–215.

Jacko S., Farkašovský R., Ďuriška I., Ščerbáková B. & Bátorová K. 2021: Critical tectonic limits for geothermal aquifer use: case study from the East Slovakian Basin Rim. *Resources* 10, 1–15. https://doi.org/10.3390/resources10040031

Janáček J. 1959: Stratigrafie, tektonika a paleogeografie východního Slovenska. In: *Geologické Práce* 52, 71–182 (in Czech).

Jerram D.A. 2001: Visual comparators for degree of grain-size sorting in two and three-dimensions. *Computers and Geosciences* 27, 485–492.

Kaličiak M. 1991: Explanatory notes to the geological map of the northern part of Slanské vrchy Mts. and Košice depression. *The State Geological Institute of Dionýz Štúr*, Bratislava, 1–231.

Karoli S. 1998: Genéza a sedimentačné prostredie evaporitov permotriasu a neogénu. Manuscript – archive. *Geological Institute of the Slovak Academy of Sciences*, Bratislava (in Slovak).

Khanin A.A. 1965: Osnovnye ucheniya o porodakhkollektorakh nefti i gaza (Main Studies of Oil and Gas Reservoir Rocks). *Publishing House Nedra*, Moscow, 1–362 (in Russian).

Khanin A.A. 1969: Porody-kollektory nefti i gaza i ikh izuchenie (Oil and Gas Reservoir Rocks and Their Study). *Publishing House Nedra*, Moscow, 1–368 (in Russian).

Koesoemadinata R.P. 1980: Geologi Minyak dan Gas Bumi. *Institut Teknologi Bandung*, 1–296 (in Indonesian).

Kováč M. 1999: Geodynamický, paleogeografický a štruktúrny vývoj karpatsko-panónskeho regiónu v miocéne. Manuscript – archive. *Geological Institute of the Slovak Academy of Sciences*, Bratislava, 1–134 (in Slovak).

Kováč M. 2000: Geodynamický, paleogeografický a štruktúrny vývoj Karpatsko-Panónskeho regiónu v miocéne: Nový pohľad na neogénne panvy Slovenska. *Veda*, Bratislava, 1–202 (in Slovak).

Kováč M. & Zlinská A. 1998: Change of paleoenvironment as a result of interaction of tectonic events and sea level oscillation in the east Slovakian Basin. *Przeglad Geologiczny* 46, 403–409.

Kováč M., Andreyeva-Grigorovich A., Bajraktarević Z., Brzobohatý R., Filipescu S., Fodor L., Harzhauser M., Nagymarosy A., Oszczypko N., Pavelić D., Rögl F., Saftić B., Sliva Ľ. & Studencka B. 2007: Badenian evolution of the Central Paratethys Sea: paleogeography, climate and eustatic sea-level changes. *Geologica Carpathica* 58, 579–606.

Kováč M., Rybár S., Halásová E., Hudáčková N., Šarinová K., Šujan M., Baranyi V., Kováčová M., Ruman A., Klučiar T. & Zlinská A. 2018: Changes in Cenozoic depositional environment and sediment provenance in the Danube Basin. *Basin Research* 30, 97–131. https://doi.org/10.1111/bre.12244

Kráľ M., Pereszlényi M. & Vass D. 1990: Vzťah rýchlosti akumulácie sedimentov ku genéze Východoslovenskej neogénnej panvy a k ložiskám uhľovodíkov. *The State Geological Institute of Dionýz Štúr*, Bratislava, 107–114 (in Slovak).

Kuthan M. 1948: Undačný vulkanizmus karpatského orogénu a vulkanologické štúdium v s. časti Prešovských hôr. *Práce Štátneho Geologického Ústavu* 17, 87–174 (in Slovak).

Lee M. & Parsons I. 2003: Microtextures of authigenic Or-rich feldspar in the Upper Jurassic Humber Group, UK North Sea. *Sedimentology* 50, 597–608. https://doi.org/10.1046/j.1365-3091.2003.00567.x

Lehotayova R. 1982: Miocene nanoplankton zones in West Carpathians. In: *Západné Karpaty* 8, 91–110.

Leško B. 1955: Geologická stavba územia medzi Vranovom a Strážskym. *Geologica Carpathica* 6, 18–42 (in Slovak).

Loeblich A.R. & Tappan H. 1992: Present status of Foraminiferal Classification. In: Takayanagi Y. & Saito T. (Eds.): Studies in Benthic Foraminifera. *Tokai University Press*, 93–102.

Łuczkowska E. 1974: Miliolidae (Foraminiferida) from the Miocene of Poland Part II. Biostratigraphy, palaeoecology, and systematics. *Acta Palaeontologica Polonica* 19, 3–176.

Martini E. 1971: Standard Tertiary and Quaternary Calcareous Nannoplankton Zonation. In: Farinacci A. (Ed.): Proceedings of the II Planktonic Conference, Roma, 1970. *Edizioni Tecnoscienza*, 739–785.

Matějka A. 1964: Vysvetlivky k prehľadnej geologickej mape ČSSR 1 : 200 000 M-34-XXII, Zborov – Košice. *The State Geological Institute of Dionýz Štúr*, Bratislava, 1–254 (in Slovak).

Merlich B. & Spitkovskaja S.M. 1974: Glubinnye razlomy, neogenovyj magmatism i orudnenje Zakarpatja. *Lvov State University*, Lvov, 1–175 (in Russian).

Miall A.D. 2006: The geology of fluvial deposits. *Springer*, New York, 1–582.

Milička J., Pereszlényi M. & Nagy A. 2011: Hydrocarbon potential of the Northern promontories of the Pannonian Basin System in Slovakia. *Mineralia Slovaca* 43, 351–364.

Morad S., Marfil R. & Peña J.A. 1989: Diagenetic K-feldspar pseudomorphs in the Triassic Buntsandstein sandstones of the Iberian Range, Spain. *Sedimentology* 36, 635–650. https://doi.org/10.1111/j.1365-3091.1989.tb02090.x

Naylor M., Mandl G. & Supesteijn C. 1986: Fault geometries in basement-induced wrench faulting under different initial stress states. *Journal of Structural Geology* 8, 737–752.

Németh K. & Martin U. 2007: Practical volcanology: lecture notes for understanding volcanic rocks from field based studies. *Occasional Papers of the Geological Institute of Hungary* 207, 1–221.

Nielsen T., Shew R.D., Steffens G.S. & Studlick J.R.J. 2007: Atlas of Deepwater Outcrops. *AAPG Studies in Geology* 56, 1–504.

Norberg N., Neusser G., Wirth R. & Harlov D. 2011: Microstructural evolution during experimental albitization of K-rich alkali feldspar. *Contributions to Mineralogy and Petrology* 162, 531–546. https://doi.org/10.1007/s00410-011-0610-y

Pellegrini C., Patruno S., Helland-Hansen W. & Steel R.J. 2020: Clinoforms and clinothems: Fundamental elements of basin infill. *Basin research* 32 185–205. https://doi.org/10.1111/bre.12446

Ptrukša pumping test: Prehľad vyčlenených obzorov na jednotlivých vrtoch, ich karotážnych výpočtových parametrov, výsledky čerpacích pokusov a ťažby. Supp.1, *Open file report*, *Geofond*, Bratislava, 1–49 (in Slovak).

Reed K.J., Janočko J., Vass D. & Gibson M. Jr. 1993: A sedimentological and petrographic investigation of the Nižný Čaj K-8 well. *Mineralia slovaca* 24, 219–226.

Repčok I. 1977: Stopy delenia uránu a možnosti ich využitia pre datovanie na príklade vulkanických skiel. *Zapadné Karpaty, Séria Mineralógia Petrografia Geochémia Ložiská* 3, 175–196 (in Slovak).

Řeřicha M. & Palšová E. 2000: Výpočet zásob zemného plynu a gazolínu na výhradnom ložisku Trhovište – Pozdišovce, stav zásob k 1.7.1997. *Open file report*, *Geofond*, No. 82816, Bratislava, 1–144 (in Slovak).

Rider M. & Kennedy M. 2011: The geological interpretation of well logs (Third Edition). *Bell and Bain*, Glasgow, 1–442.

Rossi, V., Perillo M., Steel R. & Olariu C. 2017: Quantifying mixed-process variability in shallow-marine depositional systems: What are sedimentary structures really telling us? *Journal of Sedimentary Research* 87, 1060–1074. https://doi.org/10.2110/jsr.2017.49

Rudinec R. 1960: Final well report of the Trhovište-1 well. *Open File report*, archive of NAFTA Ltd., Plavecký Štvrtok (in Slovak).

Rudinec R. 1965: Final well report of the Stretava-1 well. *Open File report*, archive of NAFTA Ltd., Plavecký Štvrtok (in Slovak).

Rudinec R. 1969a: Final well report of the Rebrín-1 well. *Open File report*, archive of NAFTA Ltd., Plavecký Štvrtok (in Slovak)

Rudinec R. 1969b: Výsledky nového štruktúrneho prieskumu v západnej časti podvihorlatskej depresie. Geologické práce, Správy 48, Bratislava. (in Slovak)

Rudinec R. 1975: Final well report of the Trhovište -26 well. *Open File report*, archive of NAFTA Ltd., Plavecký Štvrtok (in Slovak)

Rudinec R. 1976: Ložiská uhľovodíkov vo Východoslovenskom neogéne. *Mineralia Slovaca* 8, 289–384 (in Slovak).

Rudinec R. 1978: Paleogeographical, lithofacial and tectonic development of the Neogene in eastern Slovakia and its relation to volcanism and deep tectonics. *Geologica Carpathica* 29, 225–240.

Rudinec R. 1980: Možnosti výskytu ropy a plynu v predneogénnom podloží Východoslovenskej neogénnej panvy. *Mineralia Slovaca* 12, 507–531 (in Slovak).

Rudinec R. 1989: New view on the paleogeographic development of the Transcarpathian depression during the Neogene. *Mineralia Slovaca* 21, 27–42.

Rudinec R. & Čverčko J. 1970: Výsledky štruktúrneho a čiastočne pionierskeho prieskumu v podvihorlatskej oblasti so zreteľom na prieskum živíc. Manuscript – archive, *The State Geological Institute of Dionýz Štúr*, Bratislava (in Slovak).

Slavík J. 1953: Sedimentárne-petrografické výzkumy (těžké minerály) neogenních hornín východního Slovenska. In: Zpráva geologického výzkumu v roce 1952. Praha, 103–107 (in Czech).

Śliwiński M., Bąbel M., Nejbert K., Olszewska-Nejbert D., Gąsiewicz A., Schreiber B.Ch., Benowitz J.A. & Layer P. 2012: Badenian–Sarmatian chronostratigraphy in the Polish Carpathian Foredeep. *Palaeogeography, Palaeoclimatology, Palaeoecology* 326, 12–29. https://doi.org/10.1016/j.palaeo.2011.12.018

Šarinová K., Hudáčková N., Rybár S., Jamrich M., Jourdan F., Frew A., Mayers C., Ruman A., Subová V. & Sliva Ľ. 2021: $^{40}Ar/^{39}Ar$ dating and palaeoenvironments at the boundary of the early-late Badenian (Langhian–Serravallian) in the northwest margin of the Pannonian basin system. *Facies* 67, 29. https://doi.org/10.1007/s10347-021-00637-w

Spezzaferri S. 1994: Planktonic foraminiferal paleoclimatic implications across the Oligocene-Miocene transition in the oceanic record (Atlantic, Indian and South Pacific). *Palaeogeography, Palaeoclimatology, Palaeoecology* 114, 43–74. https://doi.org/10.1016/0031-0182(95)00076-X

Stamatakis M.G. 1989: A boron-bearing potassium feldspar in volcanic ash and tuffaceous rocks from Miocene lake deposits, Samos Islando Greece. *American Mineralogist* 74, 230–235.

Talling P., Masson D., Sumner E. & Malgeseni G. 2012: Subaqueous sediment density flows: Depositional processes and deposit types. *Sedimentology* 59, 1937–2003. https://doi.org/10.1111/j.1365-3091.2012.01353.x

Tari G., Horváth F. & Rumpler J. 1992: Styles of extension in the Pannonian Basin. *Tectonophysics*, 208, 203-219. https://doi.org/10.1016/0040-1951(92)90345-7

Tari G., Báldi T. & Báldi-Beke M. 1993: Paleogene retroarc flexural basin beneath the Neogene Pannonian Basin: a geodynamic model. *Tectonophysics* 226, 433–455. https://doi.org/10.1016/0040-1951(93)90131-3

Taylor T.R., Kittridge M.G., Winefield P., Bryndzia L.T. & Bonnell L.M. 2015: Reservoir quality and rock properties modeling – Triassic and Jurassic sandstones, greater Shearwater area, UK Central North Sea. *Marine and Petroleum Geology* 65, 1–21. https://doi.org/10.1016/j.marpetgeo.2015.03.020

Tschegg C., Rice H., Grasemann B., Matiasek E., Kobulej P., Dzivák M. & Berger T. 2019: Petrogenesis of a Large-Scale Miocene Zeolite Tuff in the Eastern Slovak Republic: The Nižný Hrabovec Open-Pit Clinoptilolite Mine. *Economic Geology* 114, 1177–1194. https://doi.org/10.5382/econgeo.4679

Tschegg C., Hou Z., Rice H., Fendrych J., Matiasek E., Berger T. & Grasemann B. 2020: Fault zone structures and strain localization in clinoptilolite-tuff (Nižný Hrabovec, Slovak Republic). *Journal of Structural Geology* 138, 1–14. https://doi.org/10.1016/j.jsg.2020.104090

Vass D. 1998: Geodynamic development of the Carpathian Arc in the neogene. In: Rakús M. (Ed.): Geodynamic development of the West Carpathians. *GS SR, Dionýz Štúr Publishers*, Bratislava, 155–188.

Vass D. 2002: Lithostratigraphy of Western Carpathians: Neogene and Buda Paleogene. *The State Geological Institute of Dionýz Štúr*, Bratislava, 1–202 (in Slovak).

Vass D. & Čverčko J. 1985: Litostratigrafické jednotky neogénu Východoslovenskej nížiny. *Geologické Práce* 82, 111–126 (in Slovak).

Vass D., Elečko M., Janočko J., Karoli S., Pereszlényi M., Slávik J. & Kaličiak M. 2000: Paleogeography of the East- Slovakian Basin. *Slovak Geological Magazine* 6, 377–407.

Vass D., Pereszlényi M., Soták J. & Pipík R. 2005: Geology of the East Slovakian Basin. *The State Geological Institute of Dionýz Štúr*, Bratislava, 1–65.

Vranovská A., Král M. & Vitaloš R. 2012: Geologická štúdia pre geotermálny projekt Opiná. *Čiastková správa, HG Service*, Bratislava.

Worden R.H., Griffiths J., Wooldridge L.J., Utley J.E.P., Lawan A.Y., Muhammed D.D., Simon N. & Armitage P.J. 2020: Chlorite in sandstones. *Earth-Science Reviews* 204, 1–38. https://doi.org/10.1016/j.earscirev.2020.103105

Young J.R. 1998: Neogene. In: Bown P.R. (Ed.): Calcareous Nannofossil Biostratigraphy. British Micropalaeontological Society, *Publications Series. Chapman & Hall*, London, 225–265.

Young J.R., Bown P.R. & Lees J.A. 2017: Nannotax3 website. International Nannoplankton Association (Accessed 21 Apr. 2017). http://www.mikrotax.org/Nannotax3

Zhou Q., Lv Ch., Li Ch., Chen G., Ma X. & Li Ch. 2020: Formation mechanism of authigenic chlorite in tight sandstone and its influence on tight oil adsorption, Triassic Ordos Basin, China. *Energy exploration & exploitation* 38, 2667–2694. https://doi.org/10.1177/0144598720947140

Zlinská A. 1992a: Mikrofaunistische Bewertung der Bohrung Devínska Nová Ves auf Grund der Foraminiferen und Ihre Revision. *Geologické Práce, Správy* 94, 31–34.

Zlinská A. 1992b: Zur biostratigraphischen Gliederung des Neogens des Ostslowakischen Beckens. *Geologické Práce, Správy* 96, 51–57.

Zlinská A. 1996: Mikrofauna vranovského súvrstvia z vrtu BB-1 (Byšta, Východoslovenská nížina). *Geologické Práce, Správy* 102, 37–40 (in Slovak with German summary).

Supplement

Suppl. S1: Table with results from BSE analysis – is available online at http://geologicacarpathica.com/data/files/supplements/GC-73-4-Subo-va_Suppl-S1.xlsx

Suppl. S2: Classification table of hydrocarbon reservoirs (Khanin 1965, 1969) together with classification of porosity and permeability (Koesoemadinata 1980).

	Hydrocarbon reservoirs (Khanin, 1965, 1969)			Classification of porosity and permeability (Koesoemadinata,1980)			
Class	Reservoir quality	Porosity [%]	Gas permeability [mD]	Porosity [%]	Porosity classification	Permeability [mD]	Permeability classification
VI	very low	<2	<1	0-5	very poor	<5	tight reservoir
V	low	2-8	1-10	5-10	poor	5-10	fair reservoir
IV	reduced	8-14	10-100	10-15	fair	10-100	good reservoir
III	average	14-18	100-500	15-20	good	100-1000	very good reservoir
II	high	18-20	500-1000	> 25	very good		
I	very high	≥20	≥1000				

Suppl. S3: Table with identified calcareous nannofossils and foraminifera from the Nižný Hrabovec section.

Locality	Sample	Depth [m]	Zone	Taxa (Calc.nannofoss.)	Taxa (Foraminifera)
Nižný Hrabovec section	white concretions	7.9	NN 4 or younger	***Reticulofenestra pseudoumbilicus*** *? Rhabdolithina excavata*	
Nižný Hrabovec section	**NHQ-1**	1.3-1.5	NN5-NN4	PRES ***Sphenolithus heteromorphus*** (very poor sample)	
Nižný Hrabovec section	**NHQ-2**	1.9-2.0	unassigned	***Coccolithus pelagicus*** *Reticulofenestra haqii* (single occurrences, very poor)	*Praeorbulina sicana* *Praeorbulina curva* *Orbulina suturalis*
Nižný Hrabovec section	**NHQ-3**	2.2-2.3	unassigned NN5-NN4	PRES *Triquetrorhabdulus milowii* (very poor sample)	
Nižný Hrabovec section	**NHQ-4**	2.6-2.7	unassigned	barren	
Nižný Hrabovec section	**NHQ-5**	4.3-4.6	unassigned NN5-NN4	PRES ***Reticulofenestra pseudoumbilicus*** ***Coccolithus pelagicus*** (poor sample)	
Nižný Hrabovec section	**NHQ-6**	5.8-5.9	NN 5	PRES ***Sphenolithus heteromorphus*** *Helicosphaera scissura* *Triquetrorhabdulus milowii* ***Reticulofenestra pseudoumbilicus*** *Umbilicosphaera rotula* *?Calcidiscus premacintyrei* *Reticulofenestra excavata* *Helicosphaera ampliaperta*	
Nižný Hrabovec section	**NHQ-7**	6.8-7.3	NN 5	*PRES **Sphenolithus heteromorphus*** ***Coccolithus miopelagicus*** ***Discoaster variabilis*** ***Helicosphaera mediterranea*** *Helicosphaera scissura* *Helicosphaera walbersdorfensis* *Triquetrorhabdulus milowii* *Reticulofenestra pseudoumbilicus* *Umbilicosphaera jafari* *Calcidiscus leptoporus* *Hayella challengeri*	
Nižný Hrabovec section	**NHQ-8**	8.6-8.9	NN 5	PRES ***Discoaster variabilis*** *Helicosphaera walbersdorfensis* ***Coccolithus miopelagicus*** *Reticulofenestra pseudoumbilicus* *Hayella challengeri*	
Nižný Hrabovec section	**NHQ-9**	9.8-10.1	NN 5	PRES ***Sphenolithus heteromorphus*** ***Discoaster variabilis*** *Reticulofenestra pseudoumbilicus* *?Coronocyclus nitescens* (elliptical)	
Nižný Hrabovec section	**NHQ-10**	10.7-10.8	NN 5	***Reticulofenestra pseudoumbilicus*** ***Coccolithus miopelagicus*** *Coronocyclus nitescens* (elliptical) *Calcidiscus tropicus* ***Sphenolithus heteromorphus*** *Rhabdolithina excavata* (R)	*Trilobatus bisphericus* *Orbulina universa*

Suppl. S4: Table with identified calcareous nannofossils and foraminifera from the Vranov nad Topľou section.

Locality	Sample	Depth [m]	Zone	Taxa (Calc.nannofoss.)	Taxa (Foraminifera)
Vranov nad Topľou section	VNT-1	0.5-0.6	NN 5	***Sphenolithus heteromorphus*** *Helicosphaera mediterranea* *Orthorhabdus serratus* *Calcidiscus pataecus* *Umbilicosphaera rotula* *Hayella challengeri*	*Elphidium crispum* *Elphidiella artifex* *Elphidium macellum* *Valvulineria complanata* *Bulimina pupoides* *Melonis pompilioides* *Cibicidoides pachyderma* ***Bulimina elongata*** *Cibicidoides ungerianus ornatus* *Ammonia* ex gr. *vienesis* *Asterigerina* sp. *Lobatula lobatula* *Globigerina woodi sinistral* *Trilobatus trilobus* *Trilobatus* sp. ***Orbulina suturalis***
Vranov nad Topľou section	VNT-2	1.0-1.1	NN 6	***Coronocyclus nitescens (elliptical)*** ***Discoaster variabilis*** *Discoaster deflandrei* *Discoaster* spp. *Triquetrorhabdulus milowii*	*Bolivina antiqueformis* *Globocassidulina oblonga* *Nonion commune* *Pararotalia aculeata* *Budashevaella* aff. *wilsoni* *Bathysiphon* aff. *filiformis* *Lagena pustulatostriata* *Rhabdammina* sp. *Trilobatus trilobus* *Orbulina* sp. *Elphidium* sp. *Ammonia* ex gr. *vienesis* *Valvulineria complanata* *Melonis pompilioides* ***Bulimina elongata*** *Porosononion* gr. *granosum* *Bolivina* cf. *hebes*
Vranov nad Topľou section	VNT-3	1.75-1.8	NN 6	*Coronocyclus nitescens (elliptical)* *Umbilicosphaera rotula* *Umbilicosphaera jafari* *Discoaster deflandrei* *? Discoaster exilis* *Discoaster variabilis* *Reticulofenestra pseudoumbilicus* *Sphenolithus heteromorphus* (R)	*Bucella frigida* *Vaginulina legumen* *Elphidium* sp. *Saccammina grzybowski* *Valvulineria complanata* *Bathysiphon* aff. *filiformis* *Ammonia* ex gr. *vienesis* *Bogdanowiczia pocutica* *Cibicides boueanus* *Globigerinoides trilobus* *Elphidium macellum* ***Orbulina suturalis*** *Conorbella* sp. ***Globigerina falconensis*** ***Bulimina elongata*** ***Globigerina bulloides*** *Bulimina striata mexicana* *Heterolepa* aff *dutemplei* *Porosononion* gr. *granosum* *Bulimina pupoides* *Melonis* sp.
Vranov nad Topľou section	VNT-4	1.8-3.6	NN 6	*Discoaster exilis* *Helicosphaera wallichii* *Reticulofenestra pseudoumbilicus* *Discoaster* spp. (5 ray) *Sphenolithus abies* *Calcidiscus tropicus* *Coccolithus miopelagicus* *Helicosphaera mediterranea* *Umbilicosphaera rotula* *Umbilicosphaera jafari* *Discoaster deflandrei* *Calcidiscus premacintyrei* *Sphenolithus heteromorphus* (R)	*Valvulineria complanata* *Textularia* ex gr. *gramen* *Bulimina elegans* *Spirorutilus carinatus* *Bulimina echinata* ***Orbulina suturalis*** *Bulimina elongata longa* *Globigerina* sp. indet *Heterolepa* aff *dutemplei* *Trilobatus* sp. *Nonion commune* *Globigerina regularis* sinist. *Nodosaria* sp. *Globigerina falconensis* *Porosononion granosum* *Tenuitella* sp. indet *Bolivina dilata maxima* *Cassigerinella* sp. *Bolivina antiqua* *Bolivina* sp. *Bulimina pupoides* *Neoconorbna terquemi* *Hyalinonetrion* sp. *Uvigerina bellicostata* *Uvigerina brunensis* *Cibicidoides* aff. *ungerianus* ***Globigerina bulloides*** ***Globigerina druryi*** ***Globigerina tarchanensis*** ***Globigerina praebulloides*** sinist. *Globorotalia siakensis* ***Globorotalia (Obandyella) bykovae*** *Globorotalia (Obandyella) transylvanica*

Suppl. S5: Table with identified calcareous nannofossils and foraminifera from the Trhovište-1 well.

Well	Sample Core / Box	Depth [m]	Zone	Taxa (Calc.nannofoss.)	Taxa (Foraminifera)
TRH-1	8/3	900-905	NN 5 or younger	*Coccolithus miopelagicus* *Umbilicosphaera rotula* *Umbilicosphaera jafari*	
TRH-1	15/3	1603-1606	NN 5 or younger	*Coccolithus miopelagicus* *Hayella challengeri* **Helicosphaera walbersdor- fensis**	**Bulimina elongata** **Orbulina suturalis** *Ammonia beccarii*
TRH-1	20/1	2103-2105	NN 5 or younger	*Coccolithus miopelagicus* *Orthorhabdus serratusa*	**Lagenammina atlantica**
TRH-1	21/2	2202-2204	NN 5	**Sphenolithus heteromorphus** *Sphenolithus moriformis* *Reticulofenestra pseudoum- bilicus*	**Orbulina suturalis** **Globorotalia (obandyella) bykovae** *Globigerina* sp. indet **Bogdanowiczia pocutica**
TRH-1	30/3	2649-2652	barren	*? Discoaster* spp.	
TRH-1	31/3	2649-2652	barren		
TRH-1	32/1	2752-2754			*Bathysiphon* aff. *filiformis* **Bogdanowiczia pocutica**
TRH-1	36/1	2946-2949	unassigned	*? Calcidiscus* spp. *Sphenolithus moriformis*	
TRH-1	37/1	3007-3037		*Calcidiscus tropicus* *Helicosphaera carteri*	**Orbulina suturalis** **Praeorbulina glomerosa** **Trilobatus trilobus** **Trilobatus bisphericus** **Globoturborotalita quinqueloba** *Dentoglobigerina altispira altispira* *Bulimina* sp.
TRH-1	38/1	3056-3059		*Reticulofenestra excavata*	barren

Suppl. S6: Table with identified calcareous nannofossils from the Stretava-1 well.

Well	Sample Core / Box	Depth [m]	Zone	Taxa (Calc.nannofoss.)
STR-1	44/1	2895-2898	unassigned / ?barren	*Coccolithus pelagicus* *(single occurrence)*
STR-1	45/1	2950-2953	unassigned	*Umbilicosphaera jafari* *? Syracosphaera* spp. *Pontosphaera multipora*
STR-1	49/1	3151-3153	? NN 5	*? Coccolithus miopelagicus*
STR-1	50/2	3199-3202	unassigned / NN 5-4	*Umbilicosphaera jafari* *Helicosphaera mediterranea*
STR-1	51/1	3250-3253	unassigned	*? Calcidiscus* spp.

Suppl. S7: Geological map including a time slice of the incoherence attribute with highlighted faults in the 1000 (1a, b), 2000 (2a, b) and 3000 (3a, b) milliseconds-TWT.